Landscape analysis of escape variants identifies SARS-CoV-2 spike mutations that attenuate monoclonal and serum antibody neutralization

Zhuoming Liu[1,6], Laura A. VanBlargan[2,6], Paul W. Rothlauf[1,3] Louis-Marie Bloyet[1], Rita E. Chen[2,4], Spencer Stumpf[1], Haiyan Zhao[4], John M. Errico[4], Elitza S. Theel[5], Ali H. Ellebedy[1,4], Daved H. Fremont[4], Michael S. Diamond[1,2,4,*], and Sean P. J. Whelan[1,7*]

Department of Molecular Microbiology[1], Medicine[2], Pathology & Immunology[4], School of Medicine, Washington University in St. Louis. Program in Virology[3], Harvard Medical School, Boston MA. Division of Clinical Microbiology[5], Department of Laboratory Medicine and Pathology, Mayo Clinic, Rochester, MN.

[6]These authors contributed equally

[7]Lead Contact

*Correspondence: diamond@wusm.wustl.edu (M.S.D), spjwhelan@wustl.edu (S. P. J. W.)

Figures:7

ABSTRACT

Although neutralizing antibodies against the SARS-CoV-2 spike (S) protein are a goal of most COVID-19 vaccines and being developed as therapeutics, escape mutations could compromise such countermeasures. To define the immune-mediated mutational landscape in S protein, we used a VSV-eGFP-SARS-CoV-2-S chimeric virus and 19 neutralizing monoclonal antibodies (mAbs) against the receptor binding domain (RBD) to generate 48 escape mutants. These variants were mapped onto the RBD structure and evaluated for cross-resistance by convalescent human plasma. Although each mAb had unique resistance profiles, many shared residues within an epitope, as several variants were resistant to multiple mAbs. Remarkably, we identified mutants that escaped neutralization by convalescent human sera, suggesting that some humans induce a narrow repertoire of neutralizing antibodies. By comparing the antibody-mediated mutational landscape in S protein with sequence variation in circulating SARS-CoV-2 strains, we identified single amino acid substitutions that could attenuate neutralizing immune responses in some humans.

INTRODUCTION

Control of the SARS-CoV-2 pandemic likely will require the deployment of multiple countermeasures including therapeutics and vaccines. Therapeutic candidates in development include several monoclonal antibodies (mAbs) (Baum et al., 2020a; Baum et al., 2020b; Zost et al., 2020) that recognize the SARS-CoV-2 spike (S) protein, which decorates the virion surface (Ke et al., 2020). The S protein is comprised of an N-terminal subunit (S1) that mediates receptor binding and a C-terminal subunit (S2) responsible for virus-cell membrane fusion (Wrapp et al., 2020). During viral entry into cells, the receptor-binding domain (RBD) of S1 engages the primary receptor, human angiotensin converting enzyme 2 (hACE2) (Letko et al., 2020). Processing of S by host cell proteases, typically TMPRSS2, TMPRSS4, or endosomal cathepsins, facilitates the S2-dependent fusion of viral and host-cell membranes (Hoffmann et al., 2020; Zang et al., 2020). Potently neutralizing antibodies against SARS-CoV-2 target the RBD (Baum et al., 2020b; Brouwer et al., 2020; Rogers et al., 2020; Wu et al., 2020; Zost et al., 2020) with many inhibiting infection by blocking receptor engagement (Alsoussi et al., 2020; Wu et al., 2020). Understanding the epitopes recognized by protective antibodies and whether natural variation in the S protein is associated with resistance to neutralization may predict the utility of antibody-based countermeasures.

RNA viruses exist as a swarm or “quasispecies” of genome sequences around a core consensus sequence (Dolan et al., 2018). Under conditions of selection, such as those imposed by neutralizing antibodies or drugs, variants of the swarm can escape genetically and become resistant. The relative fitness of escape mutants determines whether they are lost rapidly from the swarm or provide a competitive advantage. The intrinsically high error rates of viral RNA-dependent RNA polymerases (RdRp) result in the stochastic introduction of mutations during viral genome replication with substitutions approaching a nucleotide change per genome for each round of replication (Sanjuan et al., 2010). Coronaviruses, because of their large genome size, encode a proofreading 3'-to-5' exoribonuclease (ExoN, nsp14) that correct errors made by

the RdRp during replication (Smith and Denison, 2013). As a result of ExoN activity, the frequency of escape from antibody neutralization by coronaviruses is less than for other RNA viruses lacking such a proofreading enzyme (Smith et al., 2013).

Notwithstanding this point, to date, 2,737 mutations have been identified in the S gene of SARS-CoV-2 isolated from humans (CoV-GLUE, 2020; GISAID, 2020). These mutations give rise to 1,133 amino acid changes including 171 substitutions in the RBD. The abundance of several of these variants in the human population suggests they are not accompanied by a fitness loss. Multiple mechanisms likely account for the emergence of such substitutions including host adaptation, immune selection during natural infection, and possibly reinfection of individuals with incomplete or waning immunity. Convalescent plasma therapy, vaccination, and therapeutic antibodies could select for additional variants, and their effectiveness as countermeasures might be compromised by preexisting resistant mutants. Thus, as therapeutic antibodies and vaccines are deployed, it will be increasingly important to define the patterns of antibody resistance that arise.

Here, we used a panel of mAbs including 2B04, 1B07 and 2H04 (Alsoussi et al., 2020) and newly-generated neutralizing mAbs against SARS-CoV-2 RBD to select for escape variants and define the mutational landscape of resistance. To facilitate selection, we used a chimeric, infectious vesicular stomatitis virus (VSV) in which the endogenous glycoprotein was replaced with the S protein of SARS-CoV-2 (Case et al., 2020). VSV-eGFP-SARS-CoV-2-$S_{\Delta 21}$ (herein, VSV-SARS-CoV-2) replicates to high titer (10^7-10^8 PFU/ml within 48 h), mimics the SARS-CoV-2 requirement for human ACE2 as a receptor, and is neutralized by SARS-CoV-2 S-specific mAbs (Case et al., 2020). In two selection campaigns using 19 different mAbs, we isolated 48 different escape mutants within the RBD. Many escape mutations arose proximal to or within the ACE2 binding footprint suggesting that multiple neutralizing mAbs inhibit infection by interfering with receptor engagement. Cross-neutralization studies involving 29 of the escape mutants and 10 mAbs identified mutants that were resistant to multiple antibodies and also

those with unique resistance profiles. Remarkably, substitutions at residue E484 of S protein were associated with resistance to neutralization by polyclonal human immune sera, suggesting that some individuals generate neutralizing antibodies recognizing a focused target on the RBD. Resistance to inhibition by soluble recombinant human ACE2, a candidate decoy molecule drug (Chan et al., 2020; Monteil et al., 2020) currently in clinical trials (NCT04375046, NCT04287686), was observed with an F486S substitution. Cross-referencing of our 48 resistant mutants with sequences of clinical isolates of SARS-CoV-2 demonstrates that some single amino acid variants already circulating will be resistant to monoclonal and polyclonal antibodies. This data and functional approach may be useful for monitoring and evaluating the emergence of escape from antibody-based therapeutic and vaccine countermeasures as they are deployed.

RESULTS

Selection of mAb escape mutants in SARS-CoV-2 S.

To select for SARS-CoV-2 S variants that escape neutralization, we used VSV-SARS-CoV-2 (Case et al., 2020) and mAb 2B04 which was generated from cloned murine B cells following immunization of C57BL/6 mice with recombinant RBD and boosted with recombinant S. Antibody neutralization resistant mutants were recovered by plaque isolation (**Fig 1A**), and their resistance was verified by subsequent virus infection in the presence or absence of antibody. Antibody 2B04 failed to inhibit VSV-SARS-CoV-2 resistant variants as judged by plaque number and size (**Fig 1B**). Sequence analysis identified the mutations E484A, E484K, and F486S (**Fig 1B**), each of which fall within the RBD and map to residues involved in ACE2 binding (Lan et al., 2020) (**Fig 2**).

We extended this neutralization escape approach to nine additional inhibitory mAbs (**Fig S1, S2 and Table 1**). Sequence analysis of each isolated plaque identified multiple mutations within the RBD (**Table 2**), which we positioned on the reported crystal structure (PDB: 6M0J) (**Fig 2**): 2B04 (green), 2H04 (lime), 1B07 (blue), SARS2-01 (yellow), SARS2-02 (teal), SARS2-07 (tangerine), SARS2-16 (violet), SARS2-19 (red), SARS2-32 (fuschia), and SARS2-38 (magenta). Substitutions that led to resistance of mAbs 2B04, 1B07, SARS2-02, SARS2-07, SARS2-16, SARS2-32, and SARS2-38 cluster within and proximal to the ACE2 binding site. Resistance to antibodies SARS2-01 and SARS2-19 mapped to substitutions at sites on the side of the RBD (**Fig 2**). MAb 2H04 gave rise to resistance mutations that map exclusively on the side and the base of the RBD (**Fig 2**). The identification of resistance mutations at the side of the RBD in combination with structural data on 2H04 in complex with SARS-CoV-2 spike suggest that the mechanism of virus neutralization may be through blocking interactions with alternative attachment factors (Errico et al., in submission). The presence of resistance mutations at the base of RBD, which lie outside the 2H04 binding footprints, suggests an

allosteric mechanism of resistance, perhaps related to the ability of the RBD to adopt the up conformation requisite for ACE2 binding.

From this panel of mAbs, we observed resistance substitutions at shared positions. Four mAbs yielded substitutions at E484 (2B04, 1B07, SARS2-02, and SARS2-32), three resulted in changes to residues G446 (SARS2-02, SARS2-32, and SARS2-38) and S477 (SARS2-07, SARS2-16 and SARS2-19), and two prompted escape substitutions at F486 (2B04 and 1B07), K444 (2H04 and SARS2-38), L452 (SARS2-01 and SARS2-32), and N450 (SARS2-07 and SARS2-32), and R346 (2H04 and SARS2-01). The overlapping nature of these epitopes suggests they represent major antigenic sites within the RBD. Although amino acid changes were selected at the same position, many of the substitutions were distinct, consistent with a unique mode of binding for each antibody.

Two mAbs gave rise to variants containing linked amino acid substitutions: 2H04 (T345A and L517R) and SARS2-19 (S477N and S514F). For 2H04, substitution T345A likely arose first, as we isolated this mutation alone, and acquisition of the L517R substitution appeared to increase viral fitness as judged by plaque morphology (**Fig S2**). For SARS2-19, S477N was isolated as a single variant suggesting that this substitution arose first, however acquisition of the S514F did not alter plaque morphology (**Fig S2**). As the L517R or S514F substitutions were not identified alone, it remains unclear whether they cause resistance to 2H04 or SARS2-19 respectively. Collectively, these results show that escape mutational profiling can identify key epitopes and dominant antigenic sites.

Escape mutants confer cross-resistance to multiple mAbs.

We next evaluated whether individual mutants could escape neutralization by the other inhibitory mAbs in the panel. We tested the 29 identified escape mutants for neutralization by ten different mAbs. We defined the degree of resistance as a percentage by expressing the number of plaques formed by each mutant in the presence of antibody versus its absence. We

plotted the degree of resistance to neutralization as a heat map and arbitrarily set 50% as the cut-off value for defining resistance (**Fig 3**). Substitutions at residues T345, R346, K444, G446, N450, L452, S477, T478, E484, F486 and P499 each were associated with resistance to more than one mAb, with substitutions at S477 and E484 exhibiting broad resistance (**Fig 3**). For residues at which multiple alternate amino acids with different side chains were selected, each particular substitution was associated with a unique resistance profile. For example, K444E was resistant to SARS2-38 and 2H04 with some resistance to SARS2-1, SARS2-2 and SARS2-7, whereas K444N conferred complete resistance to SARS2-38, partial resistance to 2H04 and only weak resistance to SARS2-1 and SARS2-2. G446D was resistant to SARS2-2, SARS2-32 and SARS2-38, but G446V acquired resistance to SARS2-01. Substitutions N450K and N450Y were resistant to SARS2-01 and SARS2-32, whereas N450D facilitated resistance to SARS2-07. Substitution L452R conferred resistance to SARS2-01, SARS2-02, and SARS2-32; S477N, S477G and S477R were each highly resistant to SARS2-07, SARS2-16, and SARS2-19, and S477N and S477G result in a degree of resistance across the entire panel of antibodies; and T478I yielded resistance to SARS2-16 and SARS2-19.

Escape variants at residue E484 were isolated using 2B04, 1B07, SARS2-02, and SARS2-32, and specific substitutions at this residue led to varying degrees of resistance across the entire panel of antibodies. E484A exhibited a high degree of resistance to 2B04, 1B07, SARS2-01, SARS2-07, SARS2-19, SARS2-32, SARS2-38; E484G exhibited resistance to 2B04, 1B07, SARS2-01, SARS2-32 and SARS2-38; E484K was resistant to 2B04, 1B07, SARS2-01, SARS2-02, SARS2-16 and SARS2-32; and E484D was resistant only to 1B07 (**Fig 3 and S3**). Substitution F486S was resistant to 2B04, 1B07, SARS2-07, SARS2-16 and SARS2-19, whereas F486Y exhibited resistance only to 1B07 and SARS2-16. Finally, substitution P499L was resistant to SARS2-07, SARS2-16, and SARS2-19. In addition to demonstrating that some mutations confer resistance to multiple neutralizing mAbs, these data suggest that each mAb recognizes distinct yet partially overlapping epitopes.

Soluble human ACE2-Fc receptor decoy inhibition of escape mutants.

Soluble human ACE2 decoy receptors are under evaluation in clinical trials for treatment of COVID-19 (NCT04375046 and NCT04287686). As several of the escape mutants contain substitutions within or proximal to the ACE2 binding site, we evaluated the ability of soluble recombinant ACE2 to inhibit infection of each variant. We incubated each VSV-SARS-CoV-2 mutant with increasing concentrations of soluble human (h) or murine (m) ACE2-Fc for 1 h at 37°C and measured residual infectivity on Vero E6 cells (**Fig 4A and S4**). As observed with chimeric viruses expressing the wild-type S protein, all of the escape mutants were inhibited by hACE2-Fc but not mACE2-Fc. However, the extent of neutralization by hACE2-Fc varied (**Fig 4A**), with some mutants more sensitive to receptor inhibition and others exhibiting relative resistance. Substitutions at residues R346, A352, N450, S477, S494 and P499 were more sensitive to inhibition by soluble hACE2 than the wild-type S as evidenced by reduced IC_{50} values (**Fig 4A**) and leftward shifts of the inhibition curves (**Fig S4**). This effect was substitution-dependent as N450K was 6-fold more sensitive to hACE2 than N450Y ($P < 0.001$). Several mutants required higher (3-5-fold) concentrations of hACE2 to block infection, including substitutions at T345A, T345N, G446D, G446V, E484D and F486Y. Again, the specific substitution of a given residue impacted the effect, as T345A and T345N required higher concentrations of hACE2 to inhibit infection, whereas T345S was similar to wild type. Of the 4 substitutions observed at position E484, only E484D was less sensitive (4.6-fold, $P < 0.0001$) to hACE2 inhibition. The most striking effect was observed for F486S, where we achieved 38% inhibition at the highest concentration (20 µg/ml) of hACE2-Fc tested (**Fig 4A and B**). Residue F486 is located on the top of the hACE2 contact loop of RBD, and the presence of a large hydrophobic residue facilitates efficient receptor engagement (Lan et al., 2020; Shang et al., 2020). Although this substitution alters sensitivity to soluble ACE2 inhibition of infection, its impact on cell surface ACE2 engagement was not examined.

Escape mutants exhibit resistance to neutralization by polyclonal human immune sera.

We previously evaluated the ability of immune convalescent plasma from humans to neutralize VSV-SARS-CoV-2 and defined a strong correlation with inhibition of a clinical isolate of SARS-CoV-2 using a focus reduction neutralization test (FRNT) (Case et al., 2020). We tested four of the serum samples (13, 29, 35 and 37) from patients who had recovered from COVID-19 against our panel of escape mutants. All four sera neutralized infection of VSV-SARS-CoV-2-S displaying the wild-type S protein as we previously demonstrated. Remarkably, several of the escape mutants were resistant to neutralization at the highest concentration (1:80 initial dilution) of sera tested. All four of the substitutions at residue E484 were resistant to each of the four sera, suggesting that this is a dominant neutralizing epitope. Indeed, change at E484 was the only position that led to escape from sera 29 (**Fig 5A-B, and S5**). Four other substitutions (K444E, G446V, L452R and F490S) resulted in resistance to neutralization of sera 13, 35 and 37 (**Fig 5A and S5**). Substitutions N450D and N450Y but not N450K were resistant to sera 13 and 35. Sera 13 and 35 also did not efficiently neutralize S477G, L441R, and T478I. All four sera neutralized the single substitution S477N as well as wild-type virus (**Fig 5A-B**). Substitution S477N was sensitive to neutralization by sera 13 and 35 except in the presence of a second S514F substitution (**Fig 5A and S5**). Additional amino acid substitutions that conferred resistance to serum 13 include T345S and G446D. Substitution F486S, which altered sensitivity to soluble ACE2, escaped neutralization by serum 35 but not 13, 29 or 37. Thus, individual escape mutants can exhibit resistance to neutralization by polyclonal human convalescent sera. This observation suggests that the repertoire of antigenic sites on RBD that bind high titer neutralizing antibodies is limited in some humans.

Comparison of escape mutants with S sequence variants isolated in humans.

To broaden our analysis, we performed a second campaign of escape mutant selection using nine additional neutralizing mAbs generated against the RBD (**Fig 6, S6, S7 and Table**

232 **2**). This provided 19 additional escape mutants, bringing the total to 48. To determine whether
233 any of the 48 escape mutants we isolated represent S protein variants circulating in humans, we
234 compiled all publically available genome sequences of SARS-CoV-2. Using 161,182 genomes
235 from GISAID, we calculated the substitution frequencies throughout RBD protein (**Fig 7A**) and
236 mapped the identified residues onto RBD structure (**Fig 7B**). Of the 48 escape variants we
237 selected, 27 are present in circulating human isolates of SARS-CoV-2 (**Fig 7A**). The most
238 frequent S sequence variant seen in clinical isolates is D614G which is present in 86% of
239 sequenced isolates. The second most frequent substitution is S477N, which is present in 5.1%
240 of sequenced isolates and the dominant virus in Oceana. The penetrance of the remaining
241 substitutions among clinical isolates is relatively low, with G446V, P479S and T478I ranking 66,
242 76 and 82 of the top 100 variants in S or roughly 0.1% of sequenced variants. Collectively, this
243 analysis highlights that neutralizing mAbs against RBD can select for variants or changes at
244 positions that already exist within the human population and establishes that some substitutions
245 are present at high frequency.
246

DISCUSSION

Therapeutic mAbs, convalescent plasma, and vaccines are in clinical development as countermeasures against SARS-CoV-2. The efficacy of these strategies will be impacted by viral mutants that escape antibody neutralization. To define the landscape of mutations in the RBD associated with resistance, we selected escape mutants to 19 neutralizing mAbs that include some in clinical development. Characterization of escape mutants identified several that exhibit resistance to multiple antibodies, convalescent human sera, and soluble receptor decoys. Resistance to neutralization by serum from naturally infected humans suggests that the neutralizing response to SARS-CoV-2 in some individuals may be dominated by antibodies that recognize relatively few epitopes. Some escape mutants contain substitutions in residues at which variation already is observed in circulating human isolates of SARS-CoV-2. If a similar limited polyclonal response occurred following S protein-based vaccination, escape variants could emerge in the human population and compromise their efficacy.

From 19 different mAbs that neutralize SARS-CoV-2, we isolated 48 viral variants that escape neutralization. Selection of escape mutants was facilitated by the use of VSV-SARS-CoV-2, which we previously validated as an effective mimic of SARS-CoV-2 S protein mediated infection (Case et al., 2020). The mAbs were obtained following immunization with soluble RBD, and although some mice received a boost with stabilized S ectodomain protein, all escape substitutions map within the RBD. Multiple different mAbs led to resistance substitutions at K444, G446, N450, L452, S477, T478, P479, E484, F486 and P499, suggesting that they comprise major antigenic sites within the RBD. In earlier work, substitutions at residues K444, N450, E484 and F486 were identified using two antibodies that are in clinical development (Baum et al., 2020b), and a separate study using three different antibodies defined resistance substitutions at R346, N440, E484, F490 and Q493 (Weisblum et al., 2020).

The mutations we selected also inform the mechanism by which the different antibodies function. All of the resistance mutations we identified map within or proximal to the ACE2

binding site. Likely, the majority of the antibodies we tested neutralize infection by interfering with receptor engagement. Antibodies from human survivors also interfere with receptor engagement (Wu et al., 2020; Zost et al., 2020) suggesting it is a common mechanism of neutralization. Some of the resistance mutations from 2H04, SARS2-01 and SARS2-31 we identified map outside the ACE2 binding site including at the side and the base of the RBD. Structural studies on the mechanism by which 2B04 and 2H04 neutralize SARS-CoV-2 support inhibition by directly competing with ACE2 binding and an indirect mechanism, respectively. Direct competition with ACE2 binding is consistent with the escape mutants we selected with 2B04, and an indirect mechanism fits with the escape mutants we identified to 2H04. The structural studies on 2H04 are consistent with a mechanism of impeding interaction for alternative attachment factors (Errico et al., in submission). Our finding of an escape mutant to 2H04 located at the base of the RBD, outside the footprint of the antibody, suggests an allosteric mechanism of resistance. This mutation may affect the ability of the RBD to adopt the up conformation that is necessary for engagement of the cellular receptors perhaps shielding the epitope by maintaining the RBD in the down conformation. Further structural and functional work is required to define how different mutations promote antibody resistance and determine the mechanisms by which specific antibodies inhibit SARS-CoV-2 infection.

The relatively low genetic barrier to resistance combined with knowledge of the presence of relevant substitutions in clinical isolates suggests that effective mAb therapy likely will require a combination of at least two neutralizing antibodies (Baum et al., 2020a; Baum et al., 2020b; Du et al., 2020; Greaney, 2020; Li et al., 2020; Weisblum et al., 2020). Profiling whether different residues are associated with resistance to specific antibodies could facilitate the selection of combinations based on their non-overlapping resistance mutations. Although we isolated several escape mutants that exhibit cross-resistance to multiple antibodies, other antibodies are associated with unique and non-overlapping resistance. Resistance to such combinations could still arise through sequential escape whereby a resistant variant to one

antibody acquires resistance to a second. Sequential escape could be favored *in vivo* for two antibodies with different half-lives, or where a pre-existing resistant variant to one antibody already is circulating.

Substitution S477N, the second most abundant variant in circulating human isolates of SARS-CoV-2, led to a degree of resistance to all of the mAbs we profiled, including 2B04 and 2H04. Structures of 2B04 and 2H04 in complex with S protein highlight their mutually distinct contacts with the RBD (Errico et al., in submission). How S477N could lead to such broad resistance is of interest, given its penetrance among clinical isolates. One possible explanation may relate to changes in glycosylation at this position. Additional analysis is required to determine how broad the resistance associated with S477N is, and to probe the mechanism by which it occurs.

Substitutions at position E484 were associated with resistance to neutralization by several convalescent human sera. Four variants at this position (E484A, E484D, E484G and E484K) exhibited resistance to each of the human convalescent sera we tested. This suggests that high titer neutralizing antibodies may be directed toward a narrow repertoire of epitopes following natural infection. Substitution at position 484 is relatively uncommon among clinical isolates, with just 0.05% of sequenced strains showing any variation at this position, suggesting that variation at this position may come with an apparent fitness cost for viral replication. Despite this point, the relative resistance of the substitutions at this position to the human sera tested highlight how variants at single position can escape neutralization. Given the apparent limited breadth of the human neutralizing antibody response to natural infection, it will be important to define the epitope repertoire following vaccination and develop strategies that broaden neutralizing antibody responses. In this regard, the 48 viral mutants described here, combined with additional mutants reported in related studies (Baum et al., 2020b; Greaney, 2020; Li et al., 2020; Weisblum et al., 2020), provide a compendium of functionally relevant S

protein variants that could be used to profile sera from vaccine recipients in existing clinical trials.

Among the escape variants we selected, there were several that exhibited altered susceptibility to neutralization by soluble ACE2. Substitution F486S was particularly notable, as we were unable to attain 50% neutralization at the highest concentrations of soluble ACE2 tested (>20 μg/ml). The finding of an antibody escape mutant mapping to a critical residue within the ACE2 binding raises questions regarding possible receptor usage by viruses containing S proteins with F486S. Future studies that introduce F486S into an infectious cDNA clone of SARS-CoV-2 are needed to determine the significance of this change to hACE2 interactions *in vivo*.

Limitations of this study

Use of chimeric VSV that depends on SARS-CoV-2 S protein for entry into cells greatly facilitated the selection of 48 escape mutants. Although this chimeric VSV serves as an effective mimic of SARS-CoV-2 spike mediated entry and viral neutralization, sequence analysis of circulating human isolates reveals that 27 of those escape mutants are present in the context of infectious SARS-CoV-2. The remaining 21 variants may represent S sequences with compromised fitness in the background of SARS-CoV-2 highlighting one potential limitation of our work. Additional limitations of our study are the relatively few polyclonal human sera that we profiled against the panel of escape mutants that suggests substitutions at residue 484 are associated with resistance. Additional human sera samples at lower dilution factors may help determine the extent to which serum based neutralization of virus is affected by the escape mutants.

ACKNOWLEDGEMENTS

This study was supported by NIH contracts and grants (75N93019C00062 and R01 AI127828, R01 AI157155, and R37 AI059371) and the Defense Advanced Research Project Agency (HR001117S0019) and gifts from Washington University in Saint Louis.

AUTHOR CONTRIBUTIONS

Z.L designed and performed the experiments. L.A.V generated and validated all hybridoma-produced mAbs. P.W.R., L.M.B., R.E.C., S.S, provided experimental assistance. H.Z. and D.H.F. generated and provided purified ACE2 proteins, J.M.E mapped escape mutant. E.S.T identified and provided the human immune serum. A.H.E, generated and provided cloned versions of mAbs. Z.L., M.S.D., and S.P.J.W. analyzed data. Z.L., L.A.V., M.S.D and S.P.J.W. wrote the initial draft, with the other authors providing editing comments.

COMPETING FINANCIAL INTERESTS

MS.D. is a consultant for Inbios, Vir Biotechnology, NGM Biopharmaceuticals, and on the Scientific Advisory Board of Moderna and Immunome. The Diamond laboratory has received unrelated funding support in sponsored research agreements from Moderna, Vir Biotechnology, and Emergent BioSolutions. The Ellebedy laboratory has received unrelated funding support in sponsored research agreements from Emergent BioSolutions and funding support in sponsored research agreement from Abbvie to further develop 2B04 and 2H04 as therapeutic mAbs. A.H.E. and Washington University have filed a patent application that includes the SARS-CoV-2 antibodies 2B04 and 2H04 for potential commercial development. S.P.J.W. and Z.H.L have filed a disclosure with Washington University for VSV-SARS-CoV-2 mutants to characterize antibody panels. S. P. J. W has received unrelated funding support in sponsored research agreements with Vir Biotechnology and Abbvie.

FIGURE LEGENDS

Figure 1. VSV-SARS-CoV-2 escape mutant isolation. (**A**) Outline of escape mutant selection experiment. 2B04 and a control anti-influenza mAb were tested for neutralizing activity against VSV-SARS-CoV-2. The concentration of 2B04 added in the overlay completely inhibited viral infection (middle panel). Data are representative of two independent experiments. Plaque assays were performed to isolate the VSV-SARS-CoV-2 escape mutant on Vero E6 TMPRSS2 cells (red arrow indicated). Plaque assays with 2B04 in the overlay (*Bottom plaque in the right panel*); plaque assays without Ab in the overlay (*Top plaque in the right panel*). Data are representative images of three independent experiments. (**B**) Schematic of S gene, which underwent Sanger sequencing to identify mutations (*left panel*). For validation, each VSV-SARS-CoV-2 mutant was tested in plaque assays with or without 2BO4 in the overlay on Vero cells (*right panel*). Representative images of two independent experiments are shown.

Figure 2. Mapping of escape mutations. The surface model of RBD (from PDB 6M0J) is depicted, and contact residues of the SARS-CoV-2 RBD-hACE2 interfaces are colored in brown. Amino acids whose substitution confers resistance to each mAb in plaque assays are indicated for 2B04 (green), 2H04 (lemon), 1B07 (blue), SARS2-01 (yellow), SARS2-02 (teal), SARS2-07 (tangerine), SARS2-16 (violet), SARS2-19 (red), SARS2-32 (fuschia), and SARS2-38 (magenta). See **Figure S1 and S2**.

Figure 3. Map of cross-neutralizing activity of VSV-SARS-CoV-2 mutants. Neutralization of VSV-SARS-CoV-2 mutants was evaluated by plaque assays performed in the presence of the antibody. Degree of resistance was defined as percentage by expressing the number of plaques formed by each mutant in the presence of antibody versus its absence and is represented as a heatmap from white (low degree of resistance) to red (high degree of resistance). Representative images of two independent experiments are shown in **Figure S3**.

Figure 4. Neutralization potency of hACE2 decoy receptors against each VSV-SARS-CoV-2 mutant. (**A**) Neutralization assay of VSV-SARS-CoV-2 mutants in the presence of

hACE2-Fc. Virus was incubated with mACE2 or hACE2 at concentrations ranging from 9 ng/ml to 20 μg/ml for 1 h a 37°C and cells were scored for infection at 7.5 h post inoculation by automated microscopy. IC_{50} values were calculated for each virus-hACE2 combination from three independent experiments. (* $P < 0.05$, ** $P < 0.01$, *** $P < 0.001$, **** $P < 0.0001$ by one-way ANOVA with Dunnett's post-test; error bars indicate standard error of the mean [SEM]). (**B**) Representative neutralization curves of wild-type and F486S mutant VSV-SARS-CoV-2 with hACE2-Fc and mACE2-Fc. Error bars represent the SEM. Data are representative of three independent experiments. Neutralization curves are provided in **Figure S4**.

Figure 5. Neutralization potency of human serum against each VSV-SARS-CoV-2 mutant. (**A**) Neutralization potency of four human sera against VSV-SARS-CoV-2 mutants. IC_{50} values were calculated from three independent experiments. Neutralization potency is represented as a rainbow color map from red (most potent with low IC_{50}) to violet (less potent with high IC_{50}). LOD indicates limit of detection (1:80) (**B**) Representative neutralization curves of wild-type, S477N and E484A mutant with four different human sera. Error bars represent the SEM. Data are representative of three independent experiments. Neutralization curves are provided in **Figure S5**.

Figure 6. Mapping of additional VSV-SARS-CoV-2 escape mutants. The surface model of RBD (from PDB 6M0J) is depicted, and contact residues of the SARS-CoV-2 RBD-hACE2 interfaces were colored in brown. Amino acids whose substitution confers resistance to each mAb in the plaque assays are indicated for SARS2-21 (lime), SARS2-22 (green), SARS2-23 (blue), SARS2-31 (yellow), SARS2-34 (cyan), SARS2-55 (orange), SARS2-58 (magenta), SARS2-66 (red), and SARS2-71 (pink). See **Figure S6 and S7**.

Figure 7. Position and frequency of RBD amino acid substitutions in SARS-CoV-2. (**A**) RBD amino acid substitutions in currently circulating SARS-CoV-2 viruses isolated from humans. For each site of escape, we counted the sequences in GISAID with an amino acid change (161,182 total sequences at the time of the analysis). Variant circulating frequency is

represented as a rainbow color map from red (less circulating with low frequency) to violet (most circulating with high frequency). A black cell indicates the variant has not yet been isolated from a patient. A rainbow cell with cross indicates the variant has been isolated from a patient, but not appear in those 48 escape mutants. (**B**) Location of natural sequence variation within the RBD. The RBD is modeled as a surface representation, Variant frequency is rainbow colored as in (**A**). Black coloration indicates variation at that residue has not yet been isolated.

SUPPLEMENTARY FIGURE LEGENDS

Figure S1. Isolation of VSV-SARS-CoV-2 escape mutants by plaque assay. Related to Fig 2. (**A**) RBD-specific antibodies were tested for neutralizing activity against VSV-SARS-CoV-2. MAbs in the left panel were purified from Expi293F cells transfected with antibody expression vector (pABVec6W) expressing heavy chain V-D-J and light Chain V-J cloned from single B cells. MAbs in the right panel were from hybridomas that bound to SARS-CoV-2-infected Vero CCL81 cells by flow cytometry. Data are representative of two independent experiments. (**B**) Plaque assays were performed to isolate the VSV-SARS-CoV-2-S escape mutant on Vero E6 TMPRSS2 cells in the present of the indicated mAb in the overlay. Representative images of two independent experiments are shown.

Figure S2. Validation of selected VSV-SARS-CoV-2 mutants. Related to Fig 2. Plaque assays were performed to validate the VSV-SARS-CoV-2 mutant on Vero cells in the presence and absence of the mAb in the overlay. MAb concentrations added in the overlay were the same as those used to select the escape mutants. Representative images of two independent experiments are shown.

Figure S3. Plaque assay validation of cross-neutralization of VSV-SARS-CoV-2 mutants. Related to Fig 3. Wild-type and identified VSV-SARS-CoV-2 mutants were tested for neutralizing activity using a plaque assay with the indicated mAb in the overlay. MAb concentrations added were the same as those used to select the escape mutants. Representative images of two independent experiments are shown.

Figure S4. Neutralization of VSV-SARS-CoV-2 mutants by hACE2 decoy receptors. Related to Fig 4. hACE2-Fc or mACE2-Fc were tested for neutralizing activity against wild-type and mutant VSV-SARS-CoV-2 (n=3). Error bars represent the SEM. Data are representative of three independent experiments.

Figure S5. Neutralization of VSV-SARS-CoV-2 mutants by human sera. Related to Fig 5. Four human sera were tested for neutralization of wild-type and mutant VSV-SARS-CoV-

2 (n = 3). Error bars represent the SEM. Data are representative of three independent experiments.

Figure S6. A second neutralization escape selection campaign with nine additional mAbs. Related to Fig 6. (**A**) **Nine** additional RBD-specific antibodies were tested for neutralization activity against VSV-SARS-CoV-2. Data are representative of two independent experiments. (**B**) Plaque assays were performed to isolate the VSV-SARS-CoV-2 escape mutant on Vero E6 TMPRSS2 cells in the presence of the indicated mAb in the overlay. Representative images of six independent experiments are shown.

Figure S7. Validation of selected VSV-SARS-CoV-2 mutants. Related to Fig 6. Plaque assays were performed to validate the VSV-SARS-CoV-2 mutant on Vero cells in the presence and absence of mAb in the overlay. MAb concentration added in the overlay were the same as those used to select the escape mutants. Representative images of two independent experiments are shown.

STAR METHODS

RESOURCE AVAILABLITY

Lead Contact. Further information and requests for resources and reagents should be directed to and will be fulfilled by the Lead Contact, Sean P. J. Whelan (spjwhelan@wustl.edu).

Materials Availability. All requests for resources and reagents should be directed to and will be fulfilled by the Lead Contact author. This includes antibodies, hybridomas, viruses, and other proteins. All reagents will be made available on request after completion of a Materials Transfer Agreement.

Data and code availability. All data supporting the findings of this study are available within the paper and are available from the corresponding author upon request.

EXPERIMENTAL MODEL AND SUBJECT DETAILS

Cells. Cells were cultured in humidified incubators at 34° or 37°C and 5% CO_2 in the indicated media. Vero CCL81, Vero E6 and Vero E6-TMPRSS2 were maintained in DMEM (Corning or VWR) supplemented with glucose, L-glutamine, sodium pyruvate, and 10% fetal bovine serum (FBS). MA104 cells were propagated in Medium 199 (Gibco) containing 10% FBS. Vero E6-TMPRSS2 cells were generated using a lentivirus vector described as previously (Case et al., 2020).

VSV-SARS-CoV-2 mutants. Plaque assays were performed to isolate the VSV-SARS-CoV-2 escape mutant on Vero E6-TMPRSS2 cells with the indicated mAb in the overlay. The concentration of mAb in the overlay was determined by neutralization assays at a multiplicity of infection (MOI) of 100. Escape clones were plaque-purified on Vero-E6 TMPRSS2 cells in the presence of mAb, and plaques in agarose plugs were amplified on MA104 cells with the mAb present in the medium. Viral stocks were amplified on MA104 cells at an MOI of 0.01 in Medium 199 containing 2% FBS and 20 mM HEPES pH 7.7 (Millipore Sigma) at 34°C. Viral

498 supernatants were harvested upon extensive cytopathic effect and clarified of cell debris by
499 centrifugation at 1,000 x g for 5 min. Aliquots were maintained at -80°C.

500 **Mouse experiments.** Animal studies were carried out in accordance with the
501 recommendations in the Guide for the Care and Use of Laboratory Animals of the National
502 Institutes of Health. The protocols were approved by the Institutional Animal Care and Use
503 Committee at the Washington University School of Medicine (Assurance number A3381-01).
504 Virus inoculations were performed under anesthesia that was induced and maintained with
505 ketamine hydrochloride and xylazine, and all efforts were made to minimize animal suffering.
506 Female BALB/c mice (catalog 000651) were purchased from The Jackson Laboratory.

507

508 **METHOD DETAILS**

509 **Sequencing of the S gene.** Viral RNA was extracted from VSV-SARS-CoV-2 mutant
510 viruses using RNeasy Mini kit (Qiagen), and S was amplified using OneStep RT-PCR Kit
511 (Qiagen). The mutations were identified by Sanger sequencing (GENEWIZ).

512 **Plaque assays.** Plaque assays were performed on Vero and Vero E6-TMPRSS2 cells.
513 Briefly, cells were seeded into 6 or 12 well plates for overnight. Virus was serially diluted using
514 DMEM and cells were infected at 37°C for 1 h. Cells were cultured with an agarose overlay in
515 the presence of Ab or absence of Ab at 34°C for 2 days. Plates were scanned on a biomolecular
516 imager and expression of eGFP is show at 48 hours post-infection.

517 **Protein expression and purification.** Soluble hACE2-Fc and mACE2-Fc were
518 generated and purified as described as previously (Case et al., 2020).

519 **Monoclonal antibodies.** mAbs 2B04, 1B07 and 2H04 were described previously
520 (Alsoussi et al., 2020). Other mAbs (SARS2-01, SARS2-02, SARS2-07, SARS2-16, SARS2-19,
521 SARS2-21, SARS2-22, SARS2-23, SARS2-31, SARS2-32, SARS2-34, SARS2-38, SARS2-55,
522 SARS2-58, SARS2-66 and SARS2-71) were generated as follows. BALB/c mice were
523 immunized and boosted twice (two and four weeks later) with 5-10 μg of RBD and S protein

(twice) sequentially, each adjuvanted with 50% AddaVax and give via an intramuscular route. Mice received a final, non-adjuvanted boost of 25 μg of SARS-CoV-2 S or RBD (25 μg split via intravenous and interperitoneal routes) 3 days prior to fusion of splenocytes with P3X63.Ag.6.5.3 myeloma cells. Hybridomas producing antibodies were screened by ELISA with S protein, flow cytometry using SARS-CoV-2 infected cells, and single endpoint neutralization assays.

Human immune plasma. The human plasma samples 13, 29, 35, 37 used in this study were previously reported (Case et al., 2020), Human donor samples were collected from PCR-confirmed COVID-19 patients. Plasma samples were obtained by routine phlebotomy (Case et al., 2020). This study was approved by the Mayo Clinic Institutional Review Board.

Neutralization assays using a recombinant VSV-SARS-CoV-2. Briefly, serial dilutions of plasma beginning with a 1:80 initial dilution were three-fold serially diluted in 96-well plate over eight dilutions. Indicated dilutions of human serum were incubated with 10^2 PFU of VSV-SARS-CoV-2 for 1 h at 37 °C. Human serum-virus complexes then were added to Vero E6 cells in 96-well plates and incubated at 37 °C for 7.5 h. Cells were fixed at room temperature in 2% formaldehyde containing 10 μg/mL of Hoechst 33342 nuclear stain for 45 min. Fixative was replaced with PBS prior to imaging. Images were acquired using an In Cell 2000 Analyzer automated microscope (GE Healthcare) in both the DAPI and FITC channels to visualize nuclei and infected cells (×4 objective, 4 fields per well). Images were analyzed using the Multi Target Analysis Module of the In Cell Analyzer 1000 Workstation Software (GE Healthcare). GFP-positive cells were identified using the top hat segmentation method and counted within the InCell Workstation software. ACE2 neutralization assays using VSV-SARS-CoV-2 were conducted similarly. The initial dilution started at 20 ug/mL and was three-fold serially diluted in 96-well plates over eight dilutions. mAb neutralization assays using VSV-SARS-CoV-2were conducted similarly but using an MOI of 100.

QUANTIFICATION AND STATISTICAL ANALYSIS

All statistical tests were performed using GraphPad Prism 8.0 software as described in the indicated figure legends. Non-linear regression (curve fit) was performed to calculate IC_{50} values for **Fig 4B, 5B, S5A, and S6A** using Prism 8.0. Non-linear regression (curve fit) was performed for **Fig 1A, S1A, S2A, and S7A** using Prism 8.0. Statistical significance in data **Fig 4A** was calculated by one-way ANOVA with Dunnett's post-test using Prism 8.0. The number of independent experiments used are indicated in the relevant Figure legends.

REFERENCES

Alsoussi, W. B., Turner, J. S., Case, J. B., Zhao, H., Schmitz, A. J., Zhou, J. Q., Chen, R. E., Lei, T., Rizk, A. A., McIntire, K. M., *et al.* (2020). A Potently Neutralizing Antibody Protects Mice against SARS-CoV-2 Infection. J Immunol *205*, 915-922.

Baum, A., Ajithdoss, D., Copin, R., Zhou, A., Lanza, K., Negron, N., Ni, M., Wei, Y., Mohammadi, K., Musser, B., *et al.* (2020a). REGN-COV2 antibodies prevent and treat SARS-CoV-2 infection in rhesus macaques and hamsters. Science.

Baum, A., Fulton, B. O., Wloga, E., Copin, R., Pascal, K. E., Russo, V., Giordano, S., Lanza, K., Negron, N., Ni, M., *et al.* (2020b). Antibody cocktail to SARS-CoV-2 spike protein prevents rapid mutational escape seen with individual antibodies. Science *369*, 1014-1018.

Brouwer, P. J. M., Caniels, T. G., van der Straten, K., Snitselaar, J. L., Aldon, Y., Bangaru, S., Torres, J. L., Okba, N. M. A., Claireaux, M., Kerster, G., *et al.* (2020). Potent neutralizing antibodies from COVID-19 patients define multiple targets of vulnerability. Science *369*, 643-650.

Case, J. B., Rothlauf, P. W., Chen, R. E., Liu, Z., Zhao, H., Kim, A. S., Bloyet, L. M., Zeng, Q., Tahan, S., Droit, L., *et al.* (2020). Neutralizing Antibody and Soluble ACE2 Inhibition of a Replication-Competent VSV-SARS-CoV-2 and a Clinical Isolate of SARS-CoV-2. Cell Host Microbe.

Chan, K. K., Dorosky, D., Sharma, P., Abbasi, S. A., Dye, J. M., Kranz, D. M., Herbert, A. S., and Procko, E. (2020). Engineering human ACE2 to optimize binding to the spike protein of SARS coronavirus 2. Science *369*, 1261-1265.

CoV-GLUE (2020). http://cov-glue.cvr.gla.ac.uk/#/home.

Dolan, P. T., Whitfield, Z. J., and Andino, R. (2018). Mapping the Evolutionary Potential of RNA Viruses. Cell Host Microbe *23*, 435-446.

Du, S., Cao, Y., Zhu, Q., Yu, P., Qi, F., Wang, G., Du, X., Bao, L., Deng, W., Zhu, H., *et al.* (2020). Structurally Resolved SARS-CoV-2 Antibody Shows High Efficacy in Severely Infected Hamsters and Provides a Potent Cocktail Pairing Strategy. Cell.

584 GISAID (2020). https://www.gisaid.org/.

585 Greaney, A. J., Starr, T. N., Gilchuk, P., Zost, S. J., Binshtein, E., Loes, A. N., Hilton, S. K.,
586 Huddleston, J., Eguia, R., Crawford, K. H. D., Dingens, A. S., Nargi, R. S., Sutton, R. E.,
587 Suryadevara, N., Rothlauf, P. W., Liu, Z., Whelan, S. P. J., Carnahan,R. H., James E. Crowe,
588 Jr., and Jesse D. Bloom, J. D. (2020). Complete mapping of mutations to the SARS-CoV-2
589 spike receptor-binding domain that escape antibody recognition. bioRxiv.

590 Hoffmann, M., Kleine-Weber, H., Schroeder, S., Kruger, N., Herrler, T., Erichsen, S., Schiergens,
591 T. S., Herrler, G., Wu, N. H., Nitsche, A., *et al.* (2020). SARS-CoV-2 Cell Entry Depends on
592 ACE2 and TMPRSS2 and Is Blocked by a Clinically Proven Protease Inhibitor. Cell *181*, 271-
593 280 e278.

594 Ke, Z., Oton, J., Qu, K., Cortese, M., Zila, V., McKeane, L., Nakane, T., Zivanov, J., Neufeldt, C.
595 J., Cerikan, B., *et al.* (2020). Structures and distributions of SARS-CoV-2 spike proteins on
596 intact virions. Nature.

597 Lan, J., Ge, J., Yu, J., Shan, S., Zhou, H., Fan, S., Zhang, Q., Shi, X., Wang, Q., Zhang, L., and
598 Wang, X. (2020). Structure of the SARS-CoV-2 spike receptor-binding domain bound to the
599 ACE2 receptor. Nature *581*, 215-220.

600 Letko, M., Marzi, A., and Munster, V. (2020). Functional assessment of cell entry and receptor
601 usage for SARS-CoV-2 and other lineage B betacoronaviruses. Nat Microbiol *5*, 562-569.

602 Li, Q., Wu, J., Nie, J., Zhang, L., Hao, H., Liu, S., Zhao, C., Zhang, Q., Liu, H., Nie, L., *et al.*
603 (2020). The Impact of Mutations in SARS-CoV-2 Spike on Viral Infectivity and Antigenicity. Cell
604 *182*, 1284-1294 e1289.

605 Monteil, V., Kwon, H., Prado, P., Hagelkruys, A., Wimmer, R. A., Stahl, M., Leopoldi, A., Garreta,
606 E., Hurtado Del Pozo, C., Prosper, F., *et al.* (2020). Inhibition of SARS-CoV-2 Infections in
607 Engineered Human Tissues Using Clinical-Grade Soluble Human ACE2. Cell *181*, 905-913
608 e907.

609 Rogers, T. F., Zhao, F., Huang, D., Beutler, N., Burns, A., He, W. T., Limbo, O., Smith, C., Song,
610 G., Woehl, J., *et al.* (2020). Isolation of potent SARS-CoV-2 neutralizing antibodies and
611 protection from disease in a small animal model. Science *369*, 956-963.
612 Sanjuan, R., Nebot, M. R., Chirico, N., Mansky, L. M., and Belshaw, R. (2010). Viral mutation
613 rates. J Virol *84*, 9733-9748.
614 Shang, J., Ye, G., Shi, K., Wan, Y., Luo, C., Aihara, H., Geng, Q., Auerbach, A., and Li, F.
615 (2020). Structural basis of receptor recognition by SARS-CoV-2. Nature *581*, 221-224.
616 Smith, E. C., Blanc, H., Surdel, M. C., Vignuzzi, M., and Denison, M. R. (2013). Coronaviruses
617 lacking exoribonuclease activity are susceptible to lethal mutagenesis: evidence for
618 proofreading and potential therapeutics. PLoS Pathog *9*, e1003565.
619 Smith, E. C., and Denison, M. R. (2013). Coronaviruses as DNA wannabes: a new model for the
620 regulation of RNA virus replication fidelity. PLoS Pathog *9*, e1003760.
621 Weisblum, Y., Schmidt, F., Zhang, F., DaSilva, J., Poston, D., Lorenzi, J. C. C., Muecksch, F.,
622 Rutkowska, M., Hoffmann, H. H., Michailidis, E., *et al.* (2020). Escape from neutralizing
623 antibodies by SARS-CoV-2 spike protein variants. bioRxiv.
624 Wrapp, D., Wang, N., Corbett, K. S., Goldsmith, J. A., Hsieh, C. L., Abiona, O., Graham, B. S.,
625 and McLellan, J. S. (2020). Cryo-EM structure of the 2019-nCoV spike in the prefusion
626 conformation. Science *367*, 1260-1263.
627 Wu, Y., Wang, F., Shen, C., Peng, W., Li, D., Zhao, C., Li, Z., Li, S., Bi, Y., Yang, Y., *et al.*
628 (2020). A noncompeting pair of human neutralizing antibodies block COVID-19 virus binding to
629 its receptor ACE2. Science *368*, 1274-1278.
630 Zang, R., Gomez Castro, M. F., McCune, B. T., Zeng, Q., Rothlauf, P. W., Sonnek, N. M., Liu,
631 Z., Brulois, K. F., Wang, X., Greenberg, H. B., *et al.* (2020). TMPRSS2 and TMPRSS4 promote
632 SARS-CoV-2 infection of human small intestinal enterocytes. Sci Immunol *5*.

633 Zost, S. J., Gilchuk, P., Case, J. B., Binshtein, E., Chen, R. E., Nkolola, J. P., Schafer, A., Reidy,
634 J. X., Trivette, A., Nargi, R. S., *et al.* (2020). Potently neutralizing and protective human
635 antibodies against SARS-CoV-2. Nature *584*, 443-449.
636

Table 1. Neutralizing mAbs

mAb	Immunogen[a]	Isotype	Conc ug/mL	EC50 ng/mL[b]
2B04	RBD, S, S	Human IgG1[c]	7,630	1.46
2H04	RBD, S, S	Human IgG1[c]	6,700	279.3
1B07	RBD, S, S	Human IgG1[c]	5,200	15
SARS2-01	RBD, S, RBD	mouse IgG1	44	86
SARS2-02	RBD, S, RBD	mouse IgG1	40	7
SARS2-07	RBD, S, RBD	mouse IgG1	87	65
SARS2-16	RBD, S, S	mouse IgG1	111	27
SARS2-19	RBD, S, S	mouse IgG1	31	15
SARS2-32	RBD, S, RBD	mouse IgG1	50	23
SARS2-38	RBD, S, S	mouse IgG1	49	8
SARS2-21	RBD, S, RBD	mouse IgA	42	24
SARS2-22	RBD, S, S	mouse IgG1	25	10
SARS2-23	RBD, S, S	mouse IgG1	126	65
SARS2-31	RBD, S, S	mouse IgG1	36	28
SARS2-34	RBD, S, S	mouse IgG1	40	19
SARS2-55	RBD, S, RBD	mouse IgG1	37	10
SARS2-58	RBD, S, S	mouse IgG1	27	6
SARS2-66	RBD, S, S	mouse IgG1	44	12
SARS2-71	RBD, S, S	mouse IgG1	49	11

[a] The order of immunogens used to immunize the mice, as described in the Methods.

[b] Neutralization of SARS-CoV-2 by each mAb was assessed by focus-reduction neutralization test. The half-maximal effective concentration (EC50 value) was determined by nonlinear regression. Results are the geometric mean from three to four independent experiments.

[C] mAb was identified as mouse IgG1 and expressed as human IgG1.

Table 2. List of mutants

Campaign 1

mAb	Nucleotide	Amino Acid
2B04	A1451C	E484A
	G1450A	E484K
	T1457C	F486S
2H04	A1033G	T345A
	C1034A	T345N
	A1033T	T345S
	A1036G	R346G
	T1322G	L441R
	A1330G	K444E
	A1033G /T1550G	T345A /L517R
1B07	A1451C	E484A
	A1452C	E484D
	A1451G	E484G
	G1450A	E484K
	T1457A	F486Y
SARS2-01	A1036G	R346G
	C1055A	A352D
	T1355G	L452R
	T1480C	S494P
SARS2-02	G1337A	G446D
	G1337T	G446V
	G1450A	E484K
SARS2-07	A1348G	N450D
	A1429G	S477G
	G1430A	S477N
	C1431G	S477R
	C1496T	P499L
SARS2-16	A1429G	S477G
	G1430A	S477N
	C1431A	S477R
SARS2-19	A1429G	S477G
	G1430A	S477N
	C1433T	T478I
	G1430A /C1541T	S477N /S514F
SARS2-32	G1337A	G446D
	T1350G	N450K
	A1348T	N450Y
	T1355G	L452R
	G1450A	E484K
	T1469C	F490S
	A1330G	K444E
	G1332T	K444N

Campaign 2

mAb	Nucleotide	Amino Acid
SARS2-21	G1427A	G476D
	G1426A	G476S
	C1433T	T478I
	C1435T	P479S
	T1456C	F486L
	T1457C	F486S
SARS2-22	A1330G	K444E
	G1332T	K444N
	A1331G	K444R
	T1334G	V445G
	G1337A	G446D
SARS2-23	C1431G	S477R
	G1447T	V483F
	T1448G	V483G
	A1452C	E484D
SARS2-31	A1132G	K378E
	A1132C	K378Q
	G1223A	R408K
	G1511A	G504D
SARS2-34	A1421C	Q474P
	G1427A	G476D
	A1429G	S477G
	G1430A	S477N
	A1429C	S477R
	C1436T	P479L
SARS2-55	G1450A	E484K
SARS2-58	A1429G	S477G
	G1430T	S477I
	G1430A	S477N
	T1456G	F486V
SARS2-66	A1372C	K458Q
	A1452C	E484D
	T1468C	F490L
SARS2-71	G1427A	G476D
	A1427G	S477G
	C1433T	T478I
	A1432C	T478P
	C1436T	P479L
	T1456G	F486V

Sanger sequencing of isolated escape variants selected for by each mAb. The mutated nucleotides and residues in the RBD region of S are highlighted in red.

Fig 1

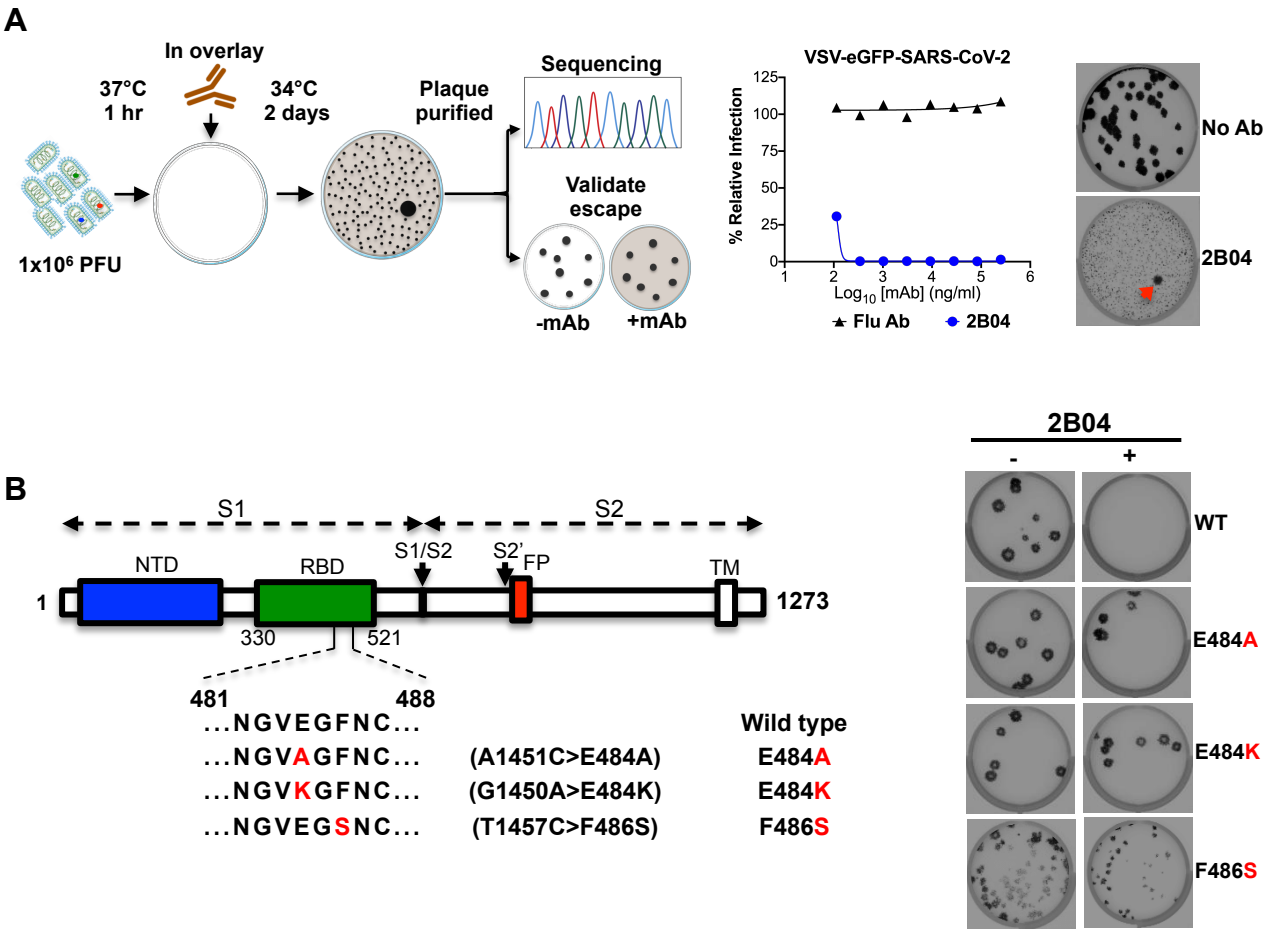
A
In overlay
37°C
1 hr
34°C
2 days
Plaque
purified
Sequencing
Validate
escape
1x10⁶ PFU
-mAb
+mAb
VSV-eGFP-SARS-CoV-2
% Relative Infection
Log10 [mAb] (ng/ml)
Flu Ab
2B04
No Ab
2B04
B
S1
S2
NTD
RBD
S1/S2
S2'
FP
TM
1
1273
330
521
481
488
...NGVEGFNC...
Wild type
...NGVAGFNC...
(A1451C>E484A)
E484A
...NGVKGFNC...
(G1450A>E484K)
E484K
...NGVEGSNC...
(T1457C>F486S)
F486S
2B04
-
+
WT
E484A
E484K
F486S

Fig 2

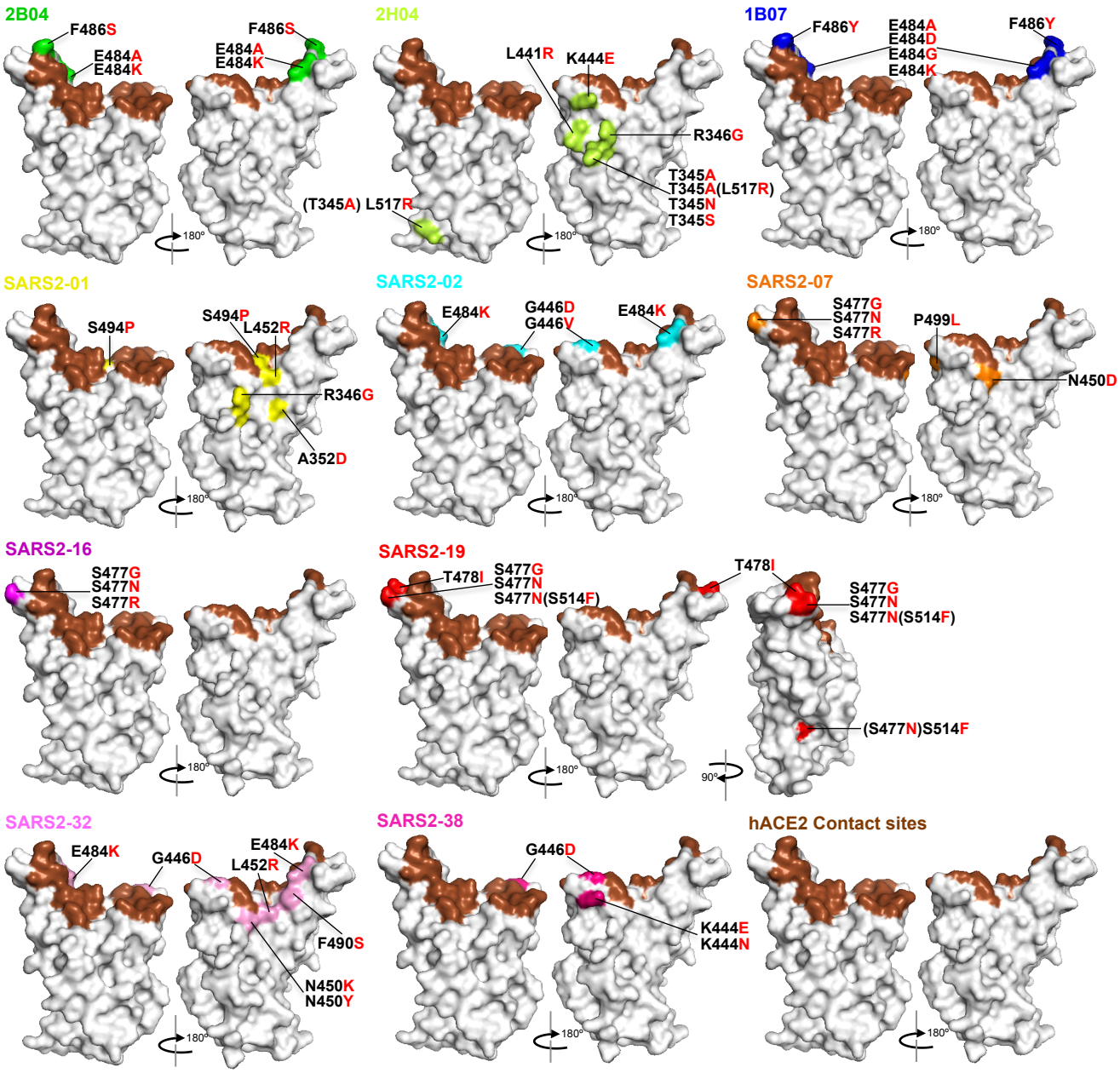
2B04
F486S
E484A
E484K
F486S
E484A
E484K
(T345A) L517R
180°
2H04
L441R
K444E
R346G
T345A
T345A(L517R)
T345N
T345S
180°
1B07
F486Y
E484A
E484D
E484G
E484K
F486Y
180°
SARS2-01
S494P
S494P
L452R
R346G
A352D
180°
SARS2-02
E484K
G446D
G446V
E484K
180°
SARS2-07
S477G
S477N
S477R
P499L
N450D
180°
SARS2-16
S477G
S477N
S477R
180°
SARS2-19
T478I
S477G
S477N
S477N(S514F)
T478I
S477G
S477N
S477N(S514F)
(S477N)S514F
180°
90°
SARS2-32
E484K
G446D
E484K
L452R
F490S
N450K
N450Y
180°
SARS2-38
G446D
K444E
K444N
180°
hACE2 Contact sites
180°

Fig 3

A

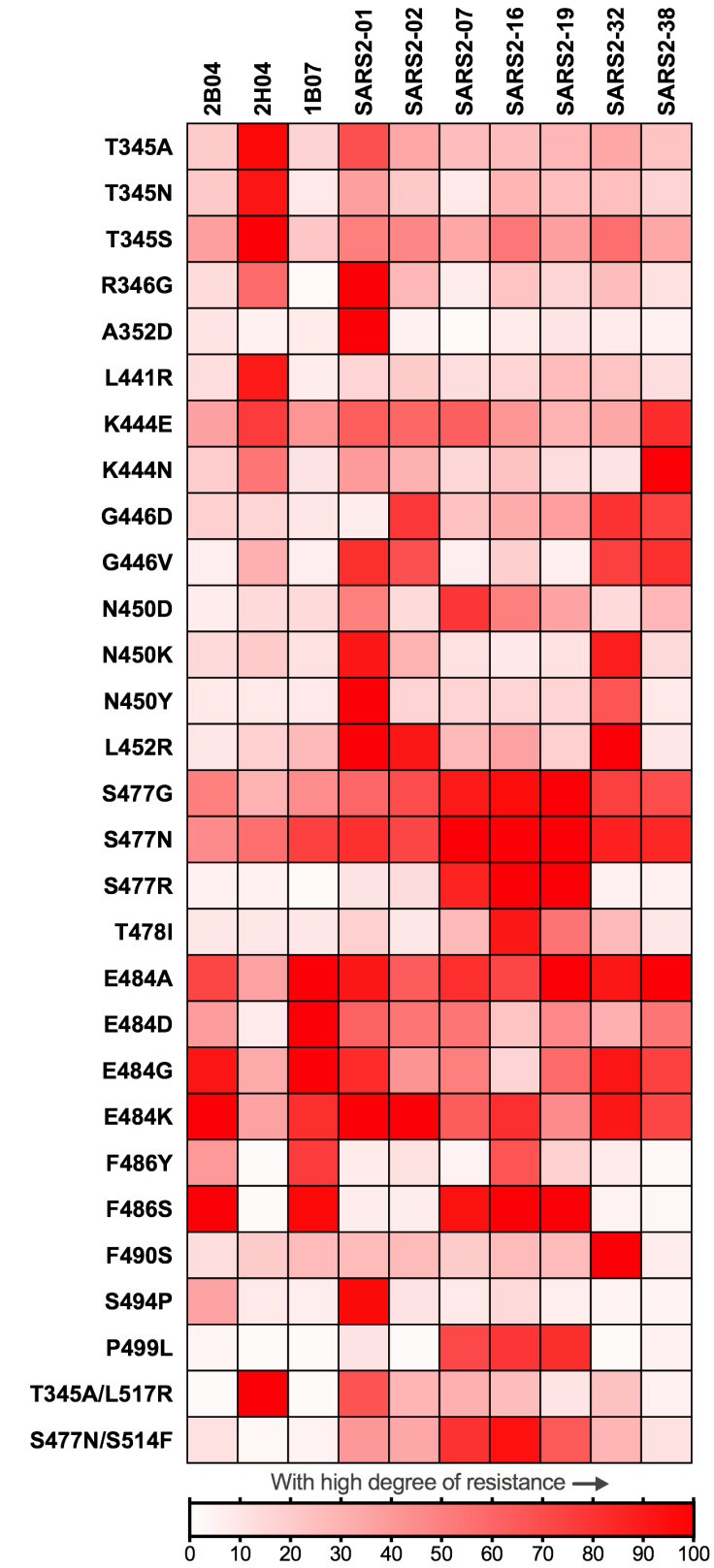
2B04
2H04
1B07
SARS2-01
SARS2-02
SARS2-07
SARS2-16
SARS2-19
SARS2-32
SARS2-38
T345A
T345N
T345S
R346G
A352D
L441R
K444E
K444N
G446D
G446V
N450D
N450K
N450Y
L452R
S477G
S477N
S477R
T478I
E484A
E484D
E484G
E484K
F486Y
F486S
F490S
S494P
P499L
T345A/L517R
S477N/S514F
With high degree of resistance
0
10
20
30
40
50
60
70
80
90
100

Fig 4

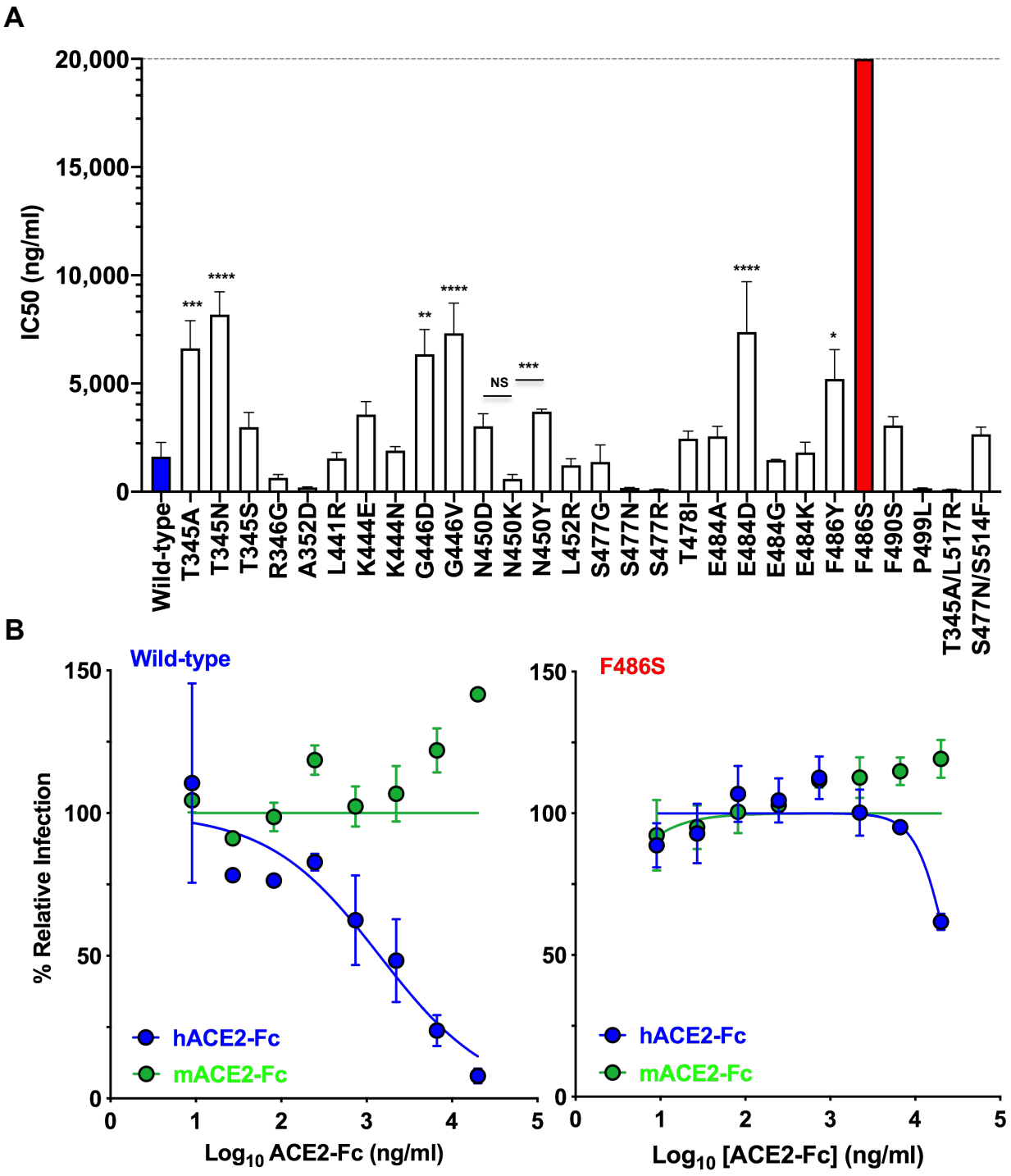
A
IC50 (ng/ml)
20,000
15,000
10,000
5,000
0
***
****
**
****
NS
***
****
*
Wild-type
T345A
T345N
T345S
R346G
A352D
L441R
K444E
K444N
G446D
G446V
N450D
N450K
N450Y
L452R
S477G
S477N
S477R
T478I
E484A
E484D
E484G
E484K
F486Y
F486S
F490S
P499L
T345A/L517R
S477N/S514F
B
Wild-type
F486S
% Relative Infection
150
100
50
0
hACE2-Fc
mACE2-Fc
0
1
2
3
4
5
Log10 ACE2-Fc (ng/ml)
Log10 [ACE2-Fc] (ng/ml)

Fig 5

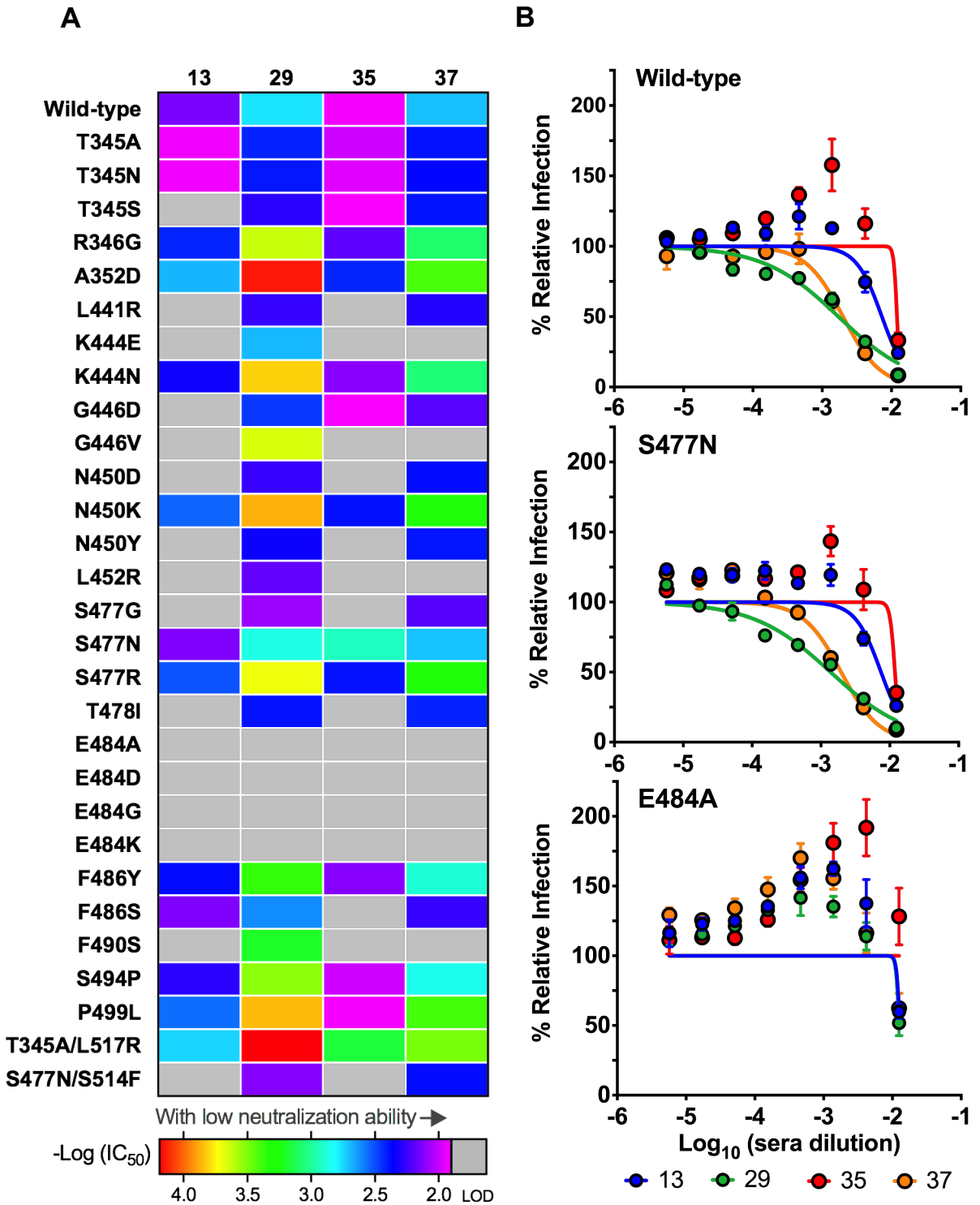
A
13
29
35
37
Wild-type
T345A
T345N
T345S
R346G
A352D
L441R
K444E
K444N
G446D
G446V
N450D
N450K
N450Y
L452R
S477G
S477N
S477R
T478I
E484A
E484D
E484G
E484K
F486Y
F486S
F490S
S494P
P499L
T345A/L517R
S477N/S514F
With low neutralization ability
-Log (IC50)
4.0
3.5
3.0
2.5
2.0
LOD
B
Wild-type
S477N
E484A
% Relative Infection
200
150
100
50
0
-6
-5
-4
-3
-2
-1
Log10 (sera dilution)
13
29
35
37

Fig 6

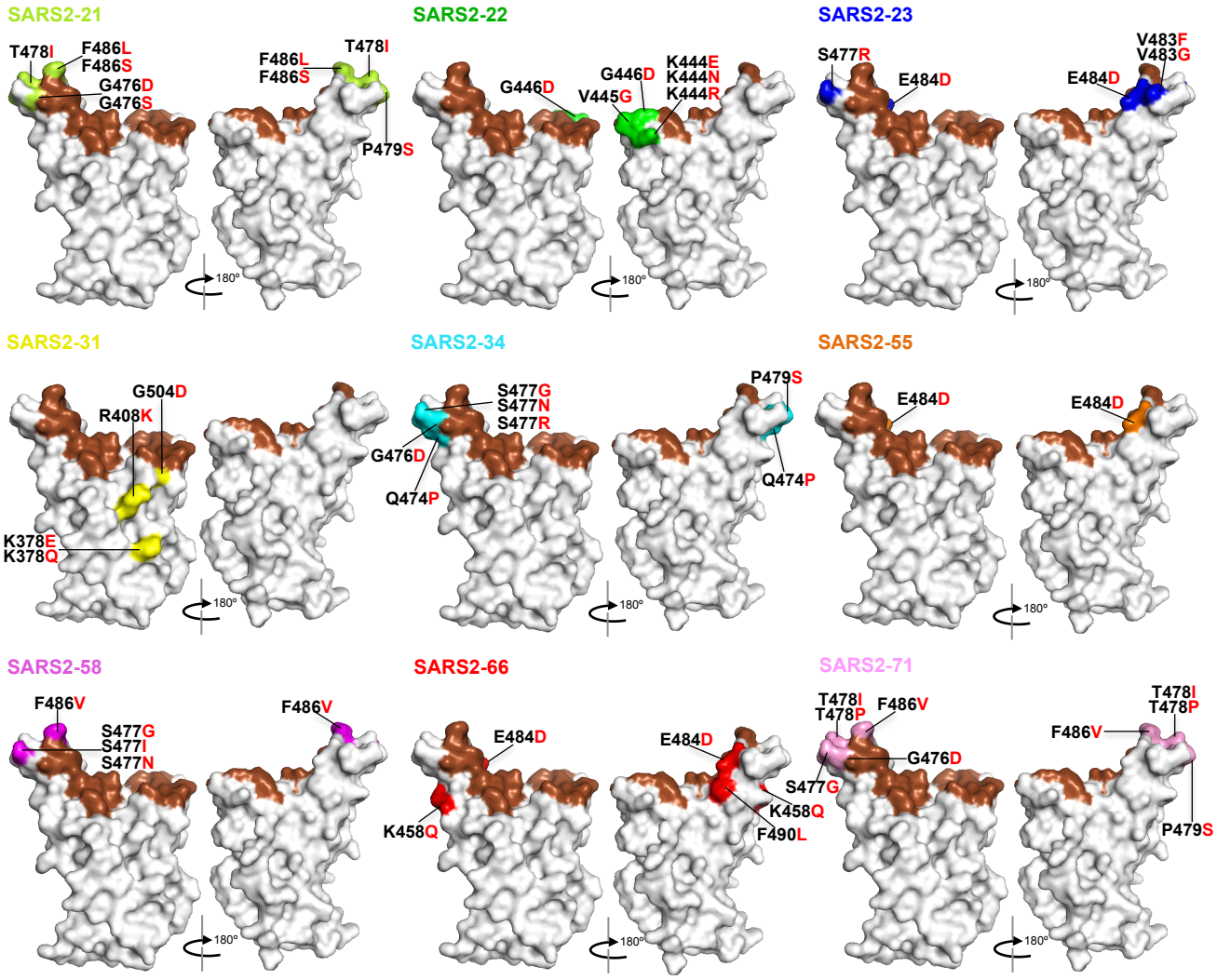
SARS2-21
T478I
F486L
F486S
G476D
G476S
F486L
F486S
T478I
P479S
180°
SARS2-22
G446D
G446D
V445G
K444E
K444N
K444R
180°
SARS2-23
S477R
E484D
V483F
V483G
E484D
180°
SARS2-31
G504D
R408K
K378E
K378Q
180°
SARS2-34
S477G
S477N
S477R
G476D
Q474P
P479S
Q474P
180°
SARS2-55
E484D
E484D
180°
SARS2-58
F486V
S477G
S477I
S477N
F486V
180°
SARS2-66
E484D
K458Q
E484D
K458Q
F490L
180°
SARS2-71
T478I
T478P
F486V
G476D
S477G
T478I
T478P
F486V
P479S
180°

Fig 7

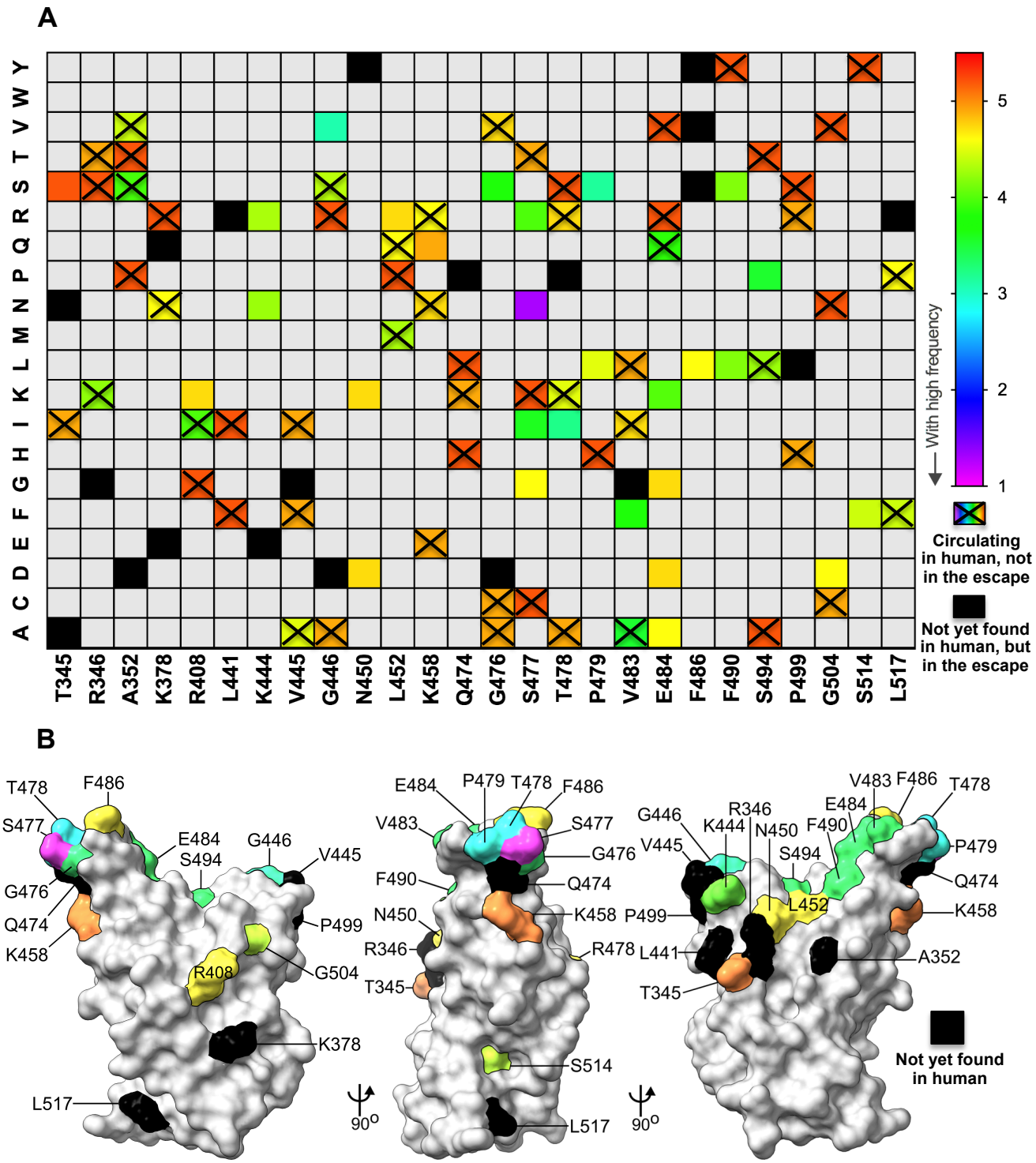
A
A C D E F G H I K L M N P Q R S T V W Y
T345 R346 A352 K378 R408 L441 K444 V445 G446 N450 L452 K458 Q474 G476 S477 T478 P479 V483 E484 F486 F490 S494 P499 G504 S514 L517
With high frequency
5
4
3
2
1
Circulating in human, not in the escape
Not yet found in human, but in the escape
B
T478 F486 S477 E484 S494 G446 V445 G476 Q474 K458 P499 R408 G504 K378 L517
E484 P479 T478 F486 V483 S477 G476 F490 Q474 N450 K458 R346 R478 T345 S514 L517
90°
V483 F486 T478 E484 G446 R346 K444 N450 F490 V445 S494 P479 Q474 P499 L452 K458 L441 A352 T345
90°
Not yet found in human

Fig S-1

A

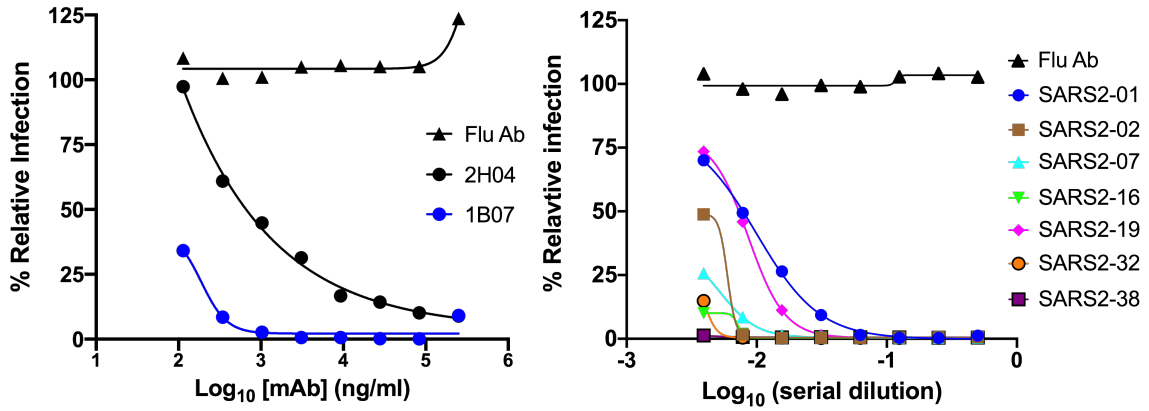
% Relative Infection
125
100
75
50
25
0
1
2
3
4
5
6
Log10 [mAb] (ng/ml)
Flu Ab
2H04
1B07
% Relavtive infection
-3
-2
-1
0
Log10 (serial dilution)
Flu Ab
SARS2-01
SARS2-02
SARS2-07
SARS2-16
SARS2-19
SARS2-32
SARS2-38

B

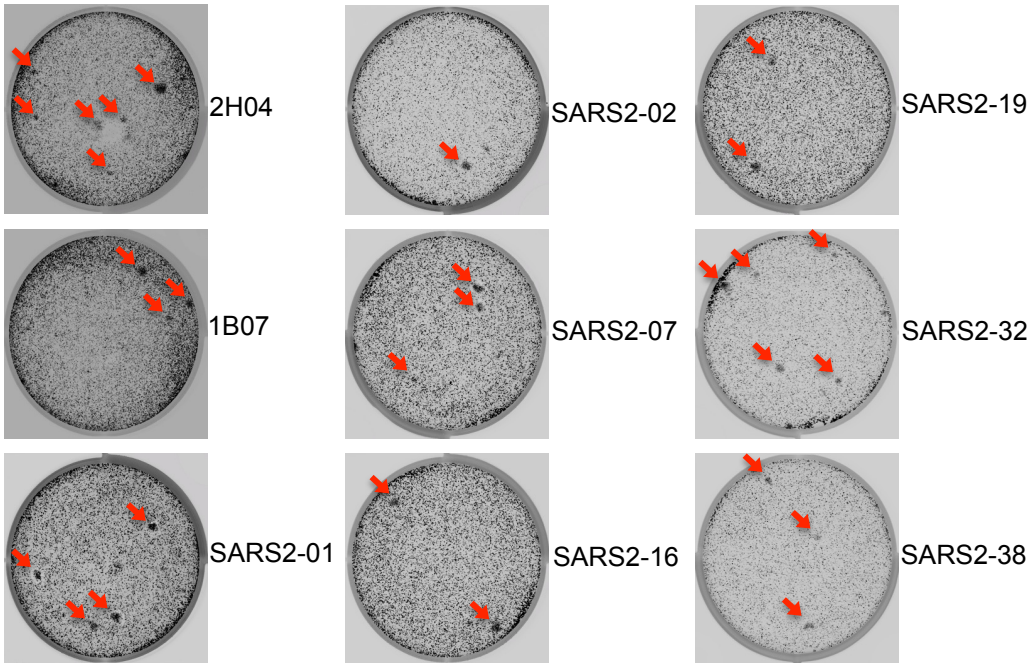
2H04
SARS2-02
SARS2-19
1B07
SARS2-07
SARS2-32
SARS2-01
SARS2-16
SARS2-38

Fig S-2

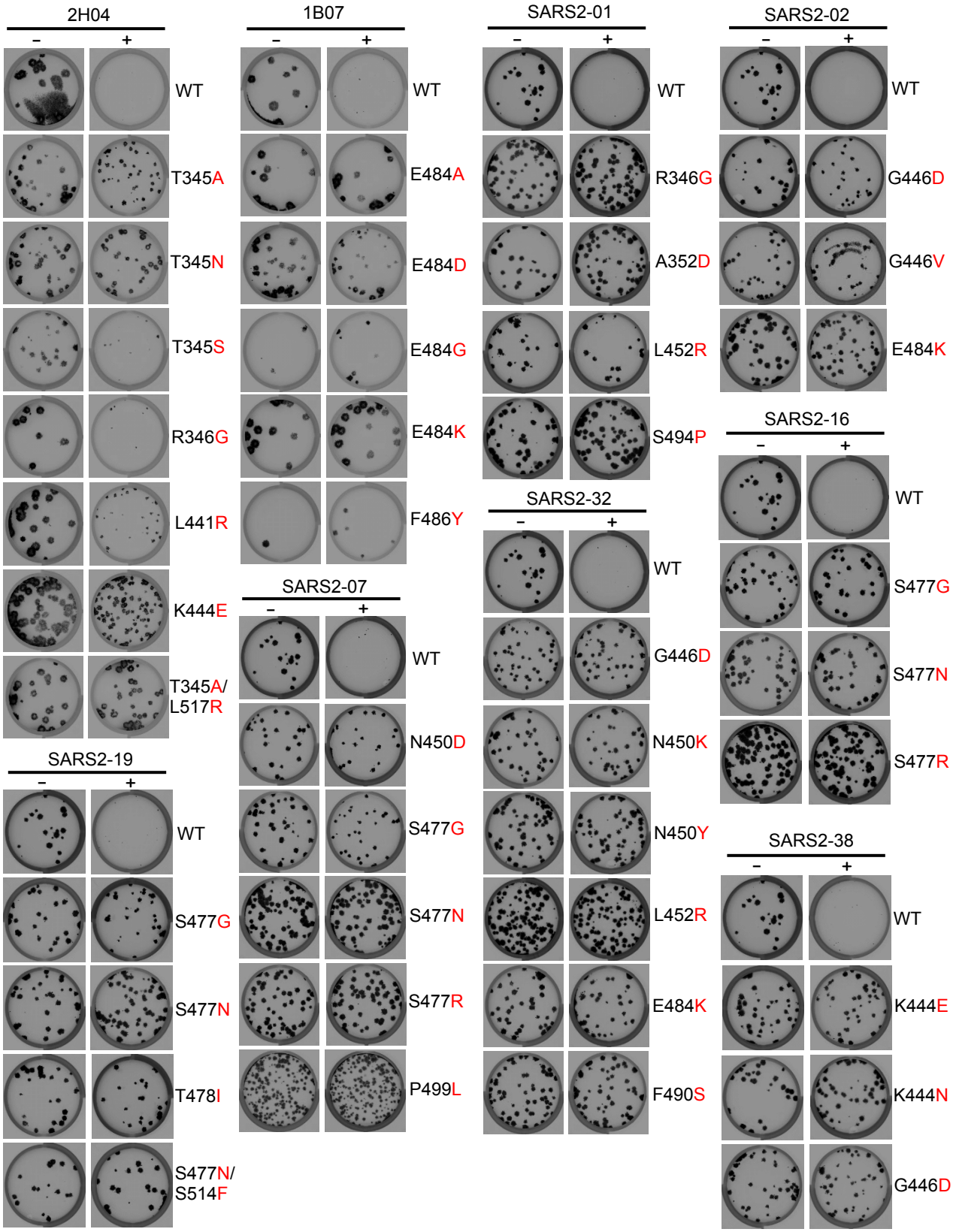
2H04
– +
WT
T345A
T345N
T345S
R346G
L441R
K444E
T345A/
L517R
1B07
– +
WT
E484A
E484D
E484G
E484K
F486Y
SARS2-07
– +
WT
N450D
S477G
S477N
S477R
P499L
SARS2-01
– +
WT
R346G
A352D
L452R
S494P
SARS2-32
– +
WT
G446D
N450K
N450Y
L452R
E484K
F490S
SARS2-02
– +
WT
G446D
G446V
E484K
SARS2-16
– +
WT
S477G
S477N
S477R
SARS2-38
– +
WT
K444E
K444N
G446D
SARS2-19
– +
WT
S477G
S477N
T478I
S477N/
S514F

Fig S-3

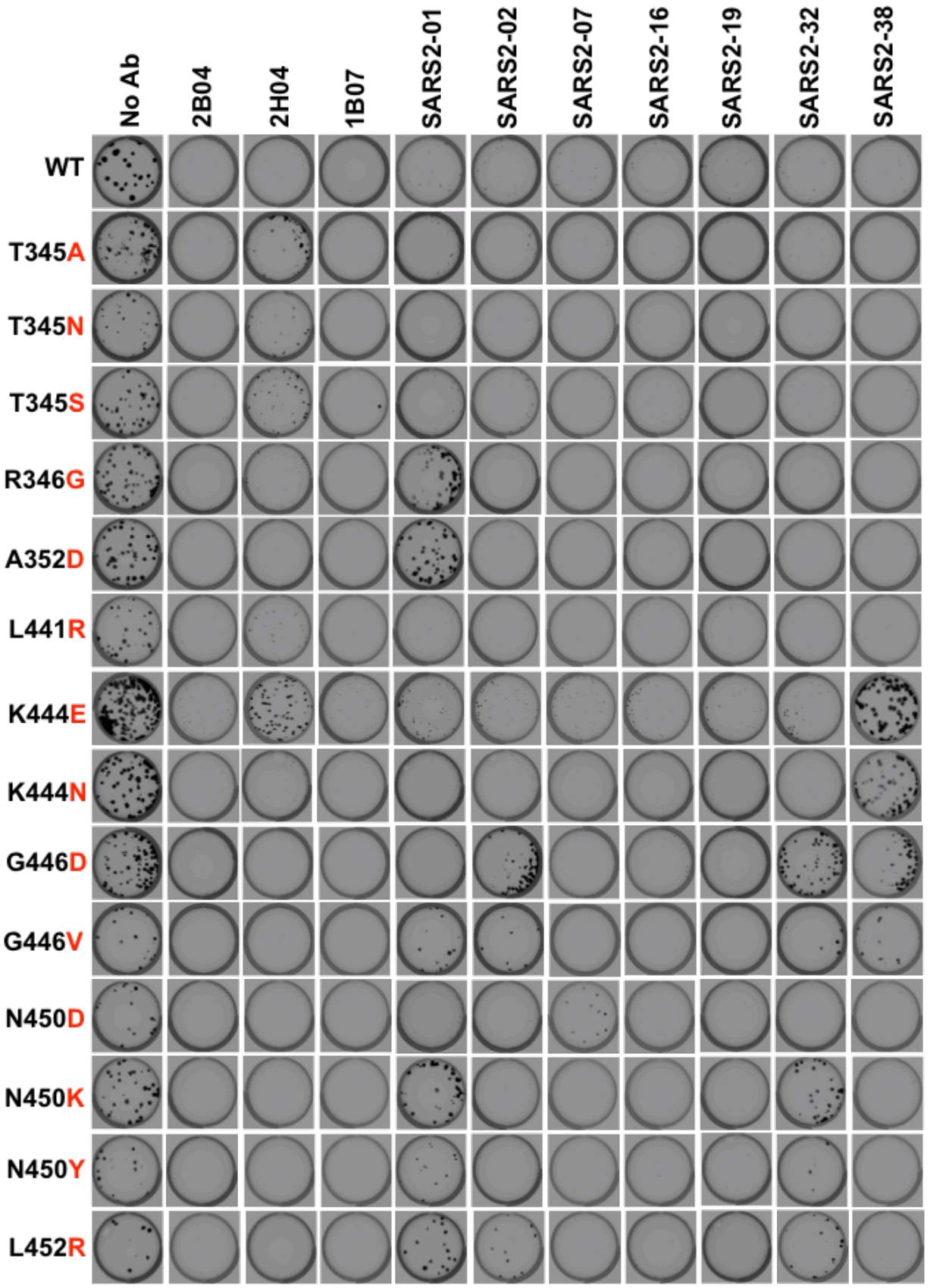
No Ab
2B04
2H04
1B07
SARS2-01
SARS2-02
SARS2-07
SARS2-16
SARS2-19
SARS2-32
SARS2-38
WT
T345A
T345N
T345S
R346G
A352D
L441R
K444E
K444N
G446D
G446V
N450D
N450K
N450Y
L452R

Fig S-3 continued

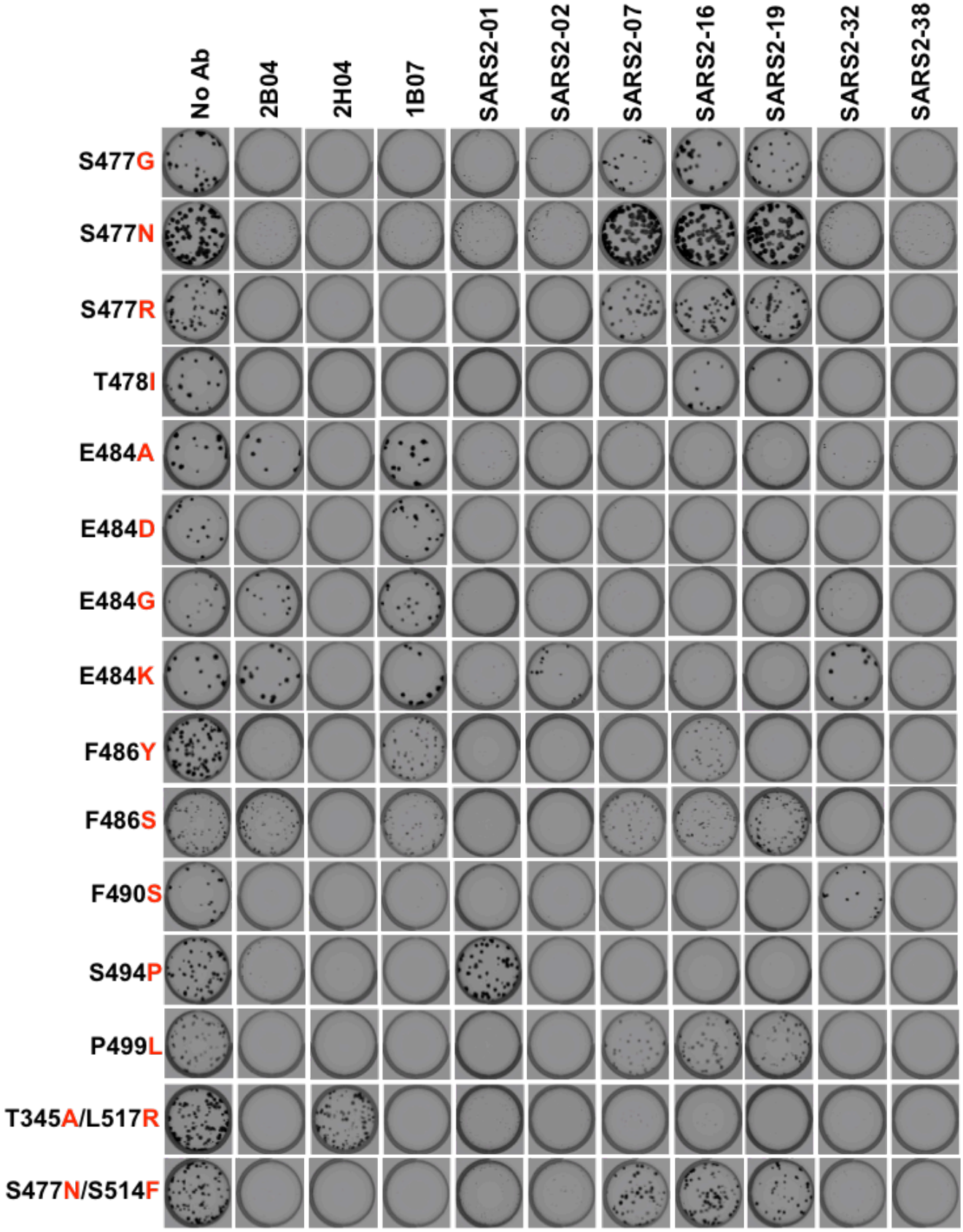

Fig S-4

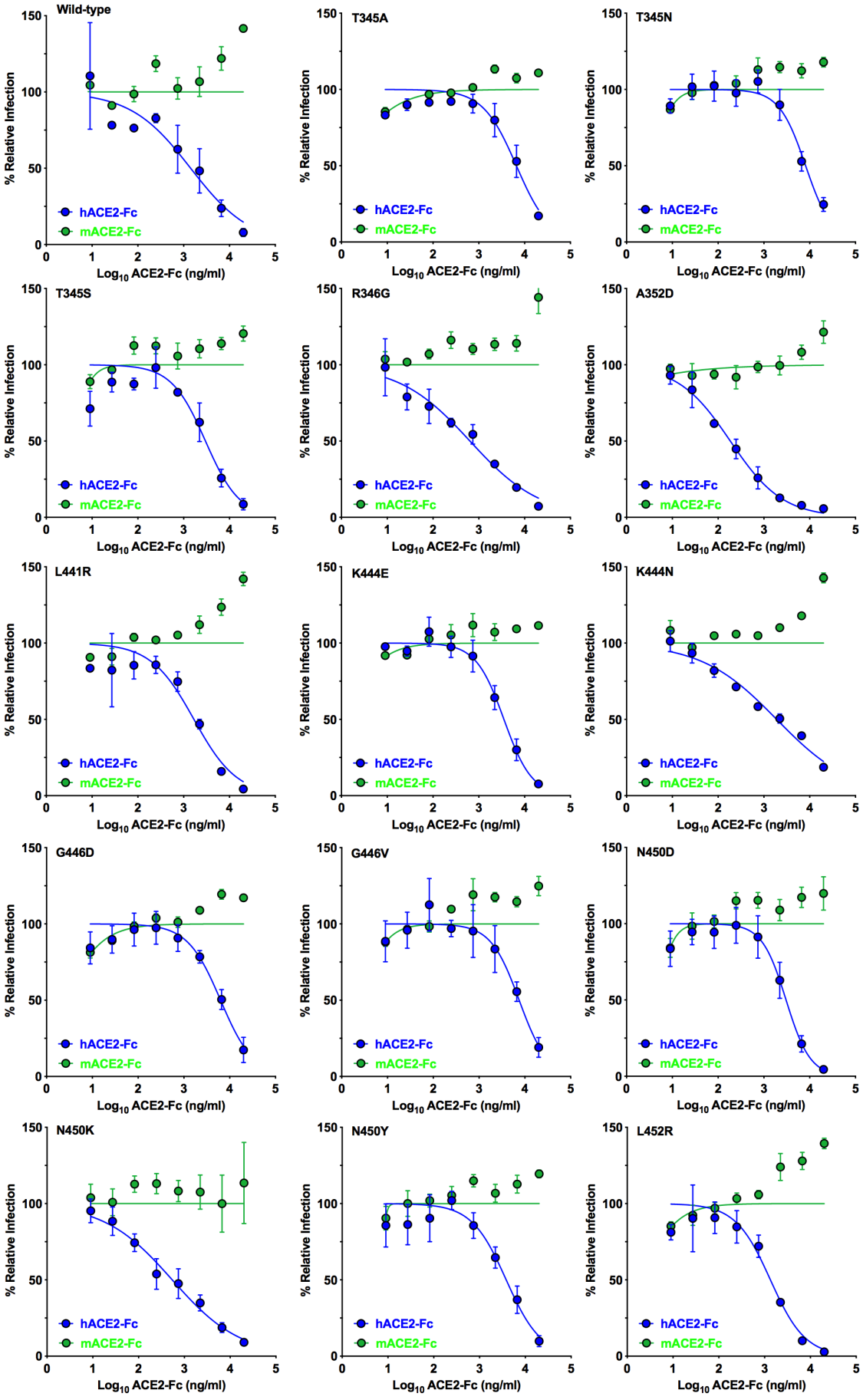
Wild-type
T345A
T345N
T345S
R346G
A352D
L441R
K444E
K444N
G446D
G446V
N450D
N450K
N450Y
L452R
% Relative Infection
Log10 ACE2-Fc (ng/ml)
hACE2-Fc
mACE2-Fc

Fig S-4 continued

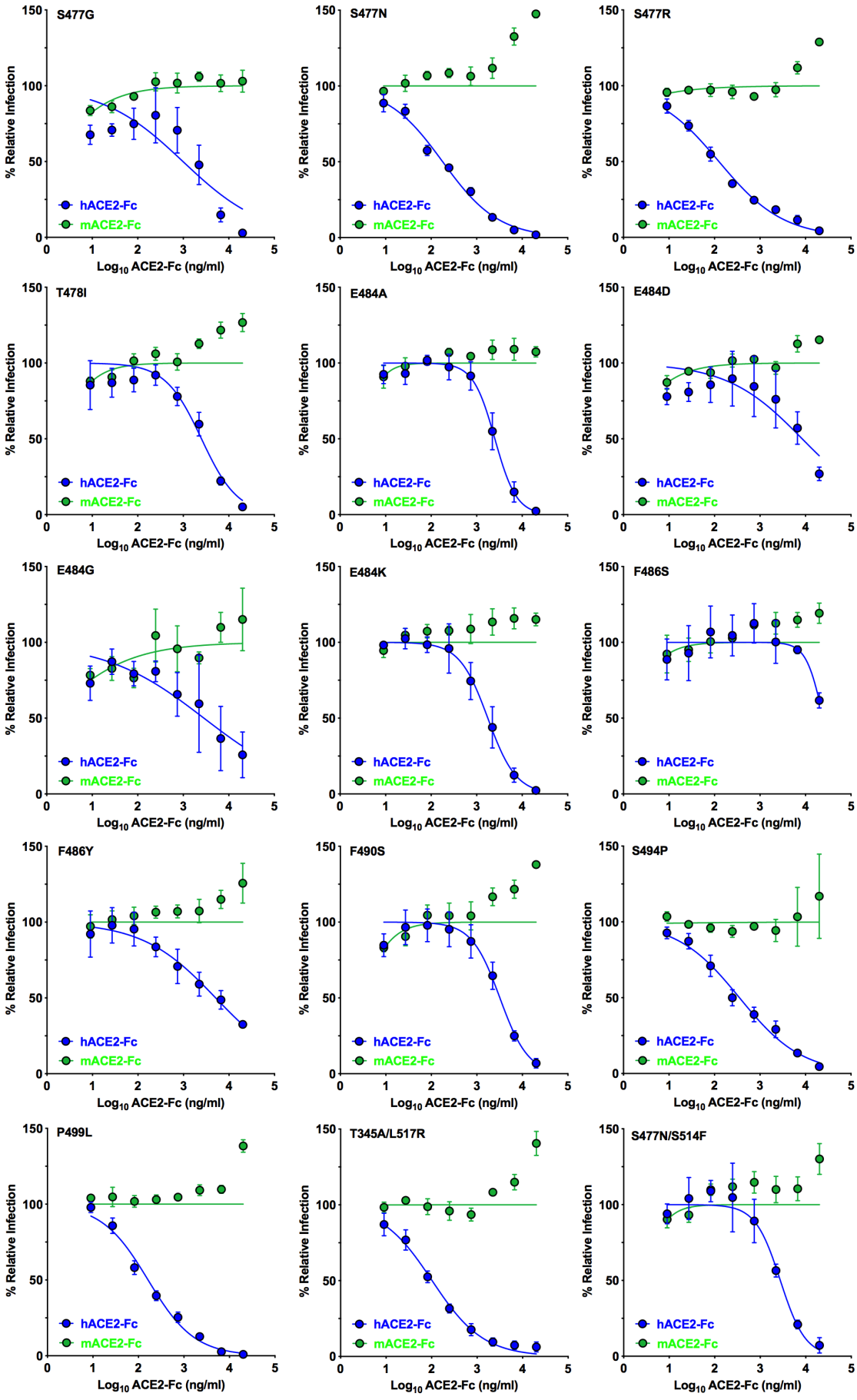

Fig S-5

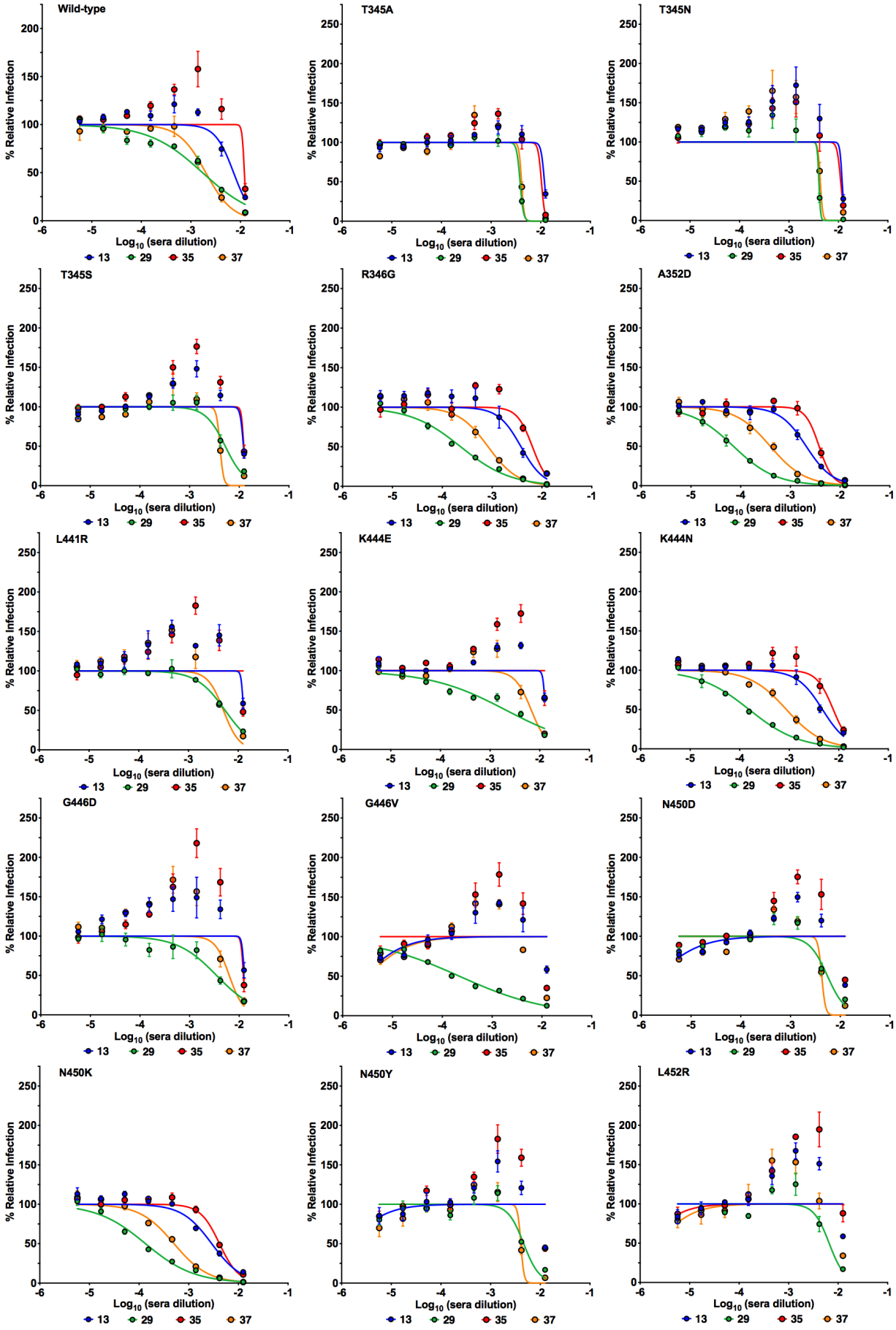
Wild-type
T345A
T345N
T345S
R346G
A352D
L441R
K444E
K444N
G446D
G446V
N450D
N450K
N450Y
L452R
% Relative Infection
Log10 (sera dilution)
13
29
35
37

Fig S-5 continued

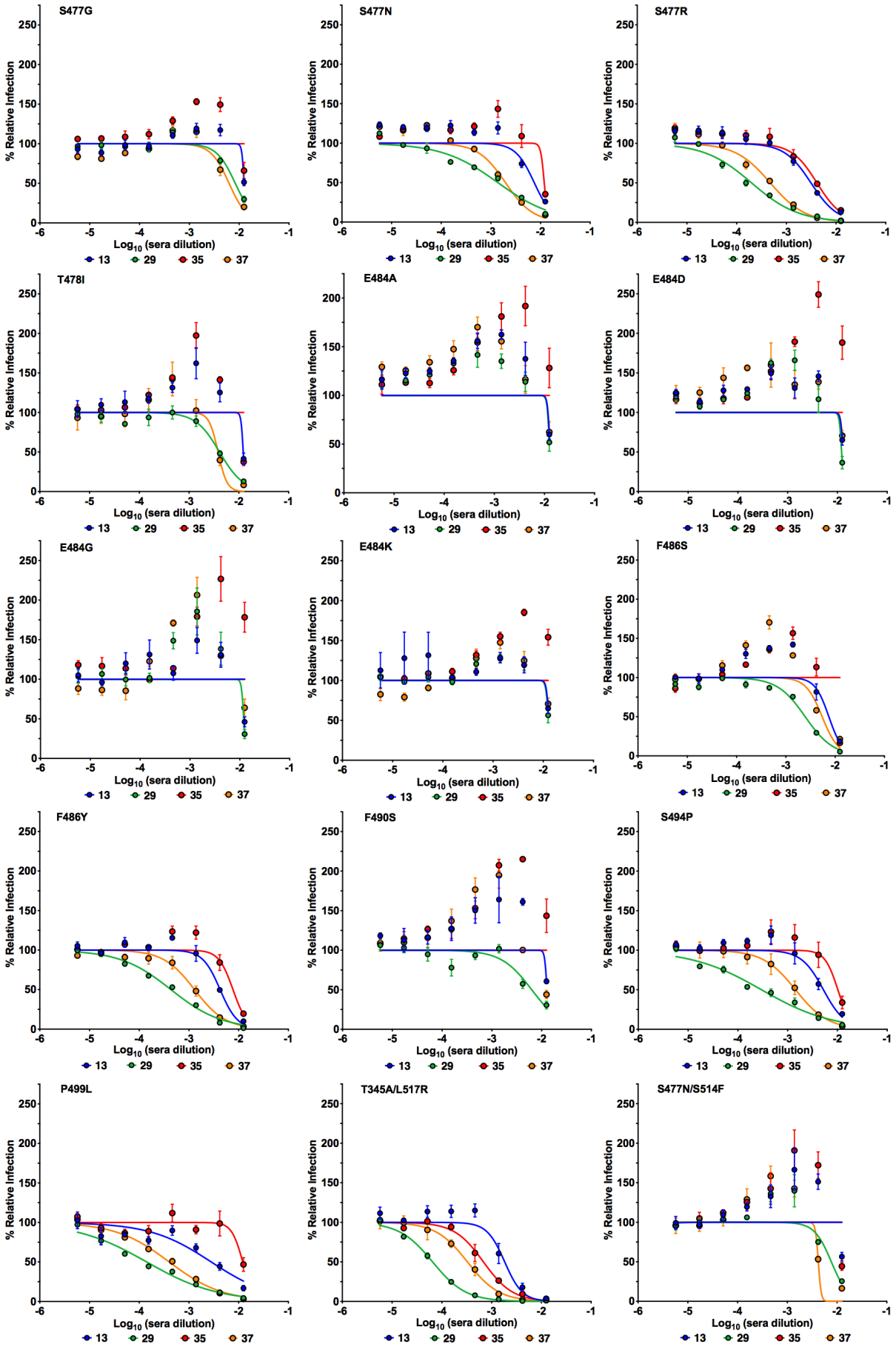

Fig S-6

A

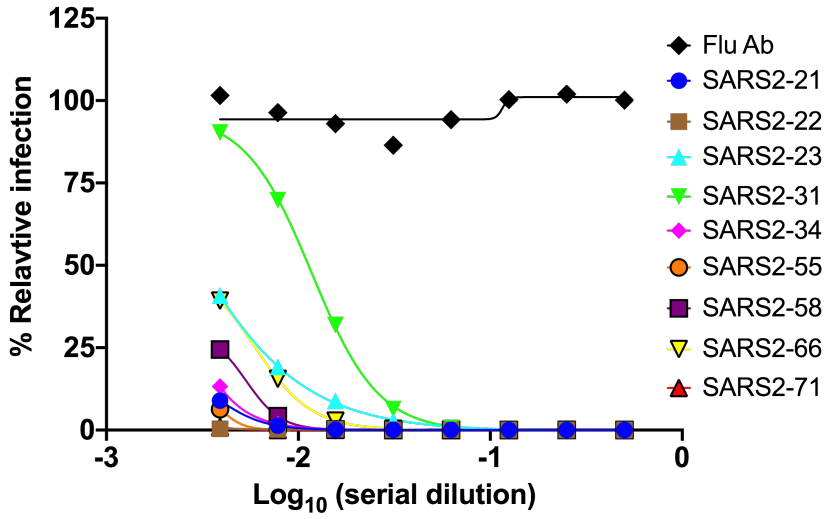
125
100
75
50
25
0
% Relavtive infection
-3
-2
-1
0
Log10 (serial dilution)
Flu Ab
SARS2-21
SARS2-22
SARS2-23
SARS2-31
SARS2-34
SARS2-55
SARS2-58
SARS2-66
SARS2-71

B

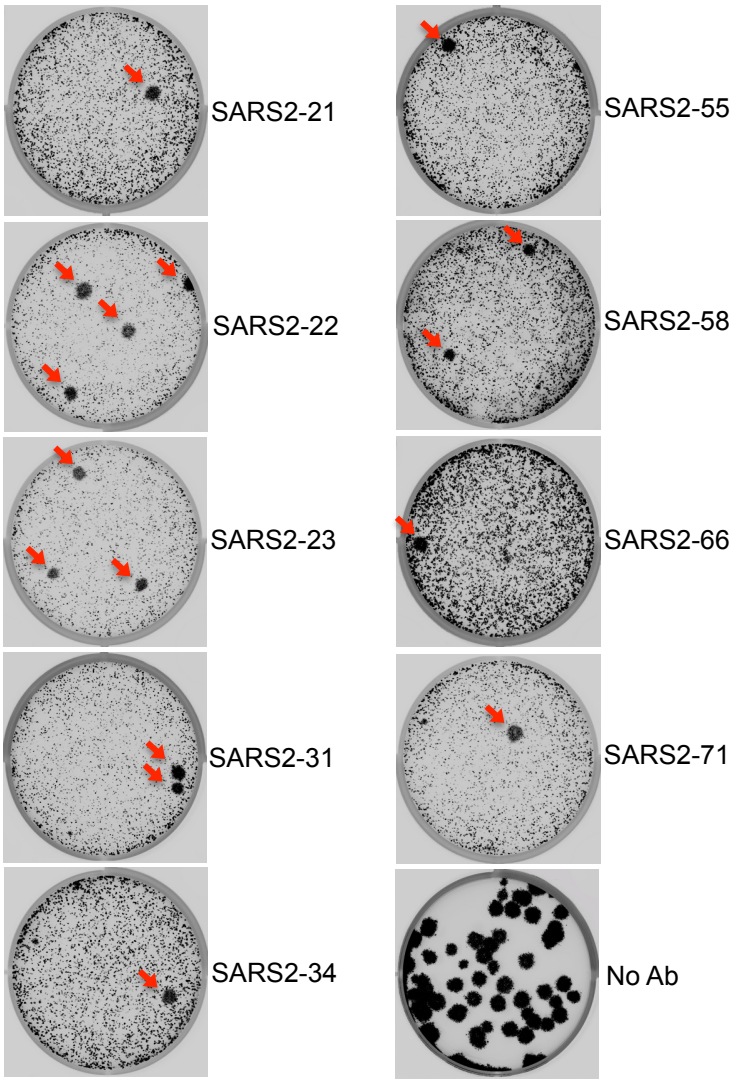
SARS2-21
SARS2-55
SARS2-22
SARS2-58
SARS2-23
SARS2-66
SARS2-31
SARS2-71
SARS2-34
No Ab

Fig S-7

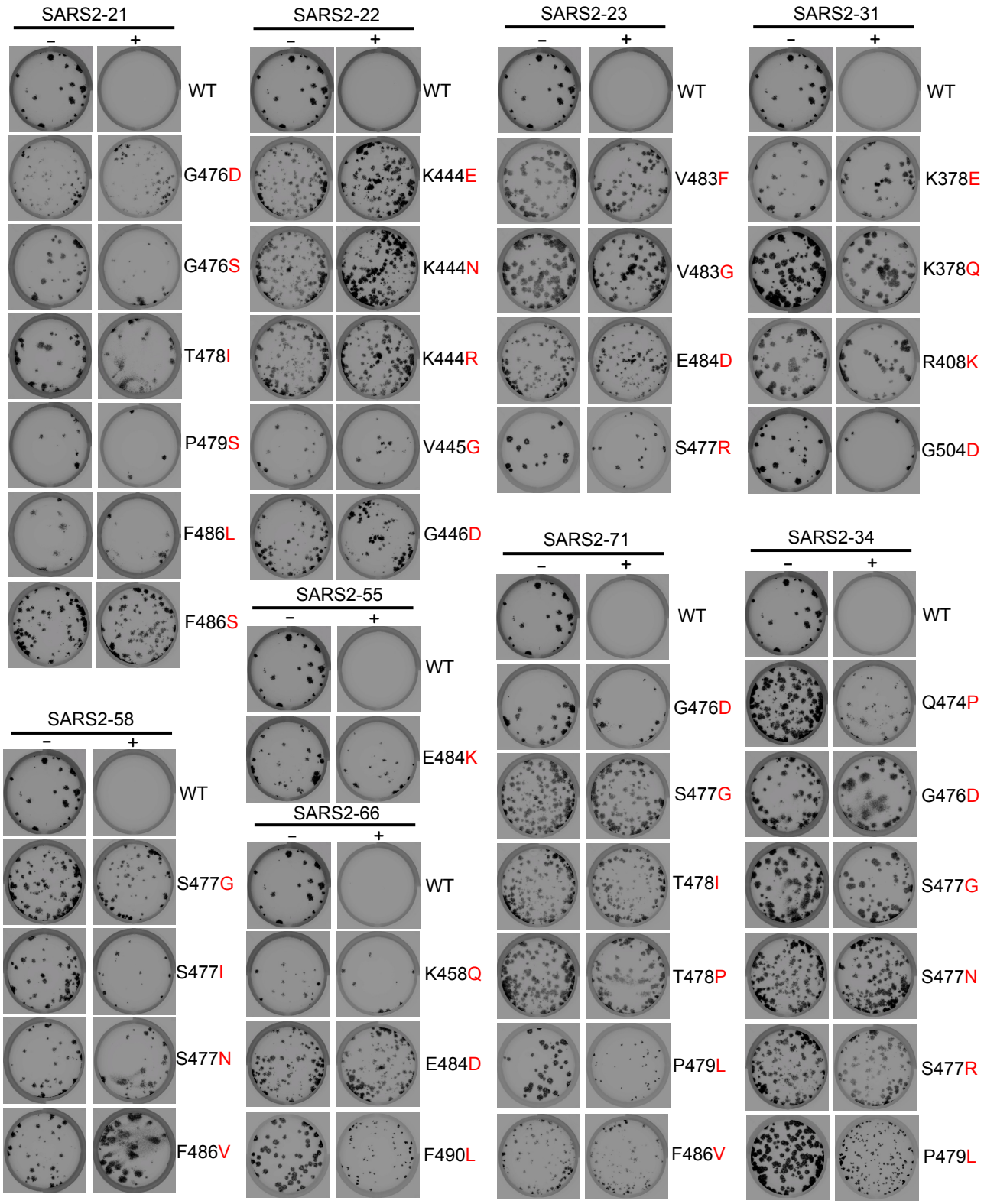
SARS2-21
SARS2-22
SARS2-23
SARS2-31
SARS2-58
SARS2-55
SARS2-66
SARS2-71
SARS2-34
WT
G476D
G476S
T478I
P479S
F486L
F486S
K444E
K444N
K444R
V445G
G446D
E484K
K458Q
E484D
F490L
V483F
V483G
E484D
S477R
K378E
K378Q
R408K
G504D
S477G
S477I
S477N
F486V
T478P
P479L
Q474P
S477R
P479L